Journal of the Geological Survey of Brazil

Composition and P-T conditions of the lithospheric mantle beneath the Azimuth 125º Lineament, Northern and Southeastern Brazil: constraints from peridotite xenoliths enclosed in diamond-bearing kimberlites

Vidyã Vieira Almeida[a*], Joseneusa Brilhante Rodrigues[b], Izaac Cabral Neto[c], Francisco Valdir Silveira[c], Homero Braz Silva[d]

[a]Geological Survey of Brazil, Geodynamics Division, Regional Superintendency for São Paulo, Rua Costa, 55, São Paulo, SP, Brazil, CEP: 01304-010
[b]Geological Survey of Brazil, Geodynamics Division, SBN, Quadra 02, Bloco H, 2º andar, Brasília, DF, Brazil, CEP: 70040-904
[c]Geological Survey of Brazil, Regional Superintendency for Recife - NANA, Rua Professor Antônio Henrique de Melo, 2010, Natal, RN, Brazil, CEP: 59078-580
[d]Brasil Explore, SHIN CA01 Lote A Salas 329, 336, Shopping Deck Norte, Lago Norte, Brasília, DF, CEP: 71503-501

Abstract

We present new petrographic and chemical data together with calculated P-T equilibrium conditions of peridotite xenoliths enclosed in kimberlites from Rondônia, Northern Brazil (Cosmos-1 and Carolina-1) and Minas Gerais, Southeastern Brazil (Canastra-1) located in the Azimuth 125º Lineament. The composition of the mantle minerals is distinct in both areas, which can be related to the diversity of the lithospheric mantle beneath the southwestern portion of the Amazonian Craton and the Brasília Belt. New and compiled chemical data indicate that subcalcic G10 garnet occurs in samples from the Canastra-1 kimberlite and other occurrences of the Alto Paranaíba Igneous Province and can be related to the remnants of the Archean lithospheric mantle of the São Francisco Craton beneath the area. The garnets from Rondônia are mostly G5 (pyroxenitic) and G9 (lherzolitic) with a higher abundance of G3 (eclogitic) and G4 (pyroxenitic/eclogitic) relative to the Alto Paranaíba Igneous Province. Higher pressures and temperatures were calculated for the samples from Rondônia (40-60 kbar and 1030-1380 ºC) compared to samples from Minas Gerais (25-40 kbar and 730-1000 ºC). The peridotite xenoliths from Rondônia show P-T equilibrium conditions in the diamond stability field and can be the source of at least part of the diamond from the area. The P-T stability fields of the xenoliths from both locations are aligned close to the 40 mW/m^2 geotherm. The data indicate that the cratonic 40 mW/m^2 geothermal gradient in Rondônia may be related to a process of thermal relaxation of the lithospheric mantle after the Paleoproterozoic to Mesoproterozoic tectonothermal events of the southwestern Amazonian Craton until the sampling of the xenoliths by the magma in the Permian-Triassic.

Article Information

Publication type: Research Papers
Received 3 August 2022
Accepted 19 October 2022
Online pub. 26 October 2022
Editor: Chris Harris

Keywords:
Subcontinental Lithospheric Mantle;
Azimuth 125º Lineament;
Mantle xenoliths;
Geothermal gradients

*Corresponding author
Vidyã Vieira Almeida
vidya.almeida@sgb.gov.br

1. Introduction

The composition of the subcontinental lithospheric mantle (SCLM) beneath igneous provinces is closely related to the chemical and isotopic signatures inherited by magmas and related mineral deposits (e.g., Marques et al. 2016; Holwell et al. 2019; Hutchison et al. 2021). The igneous provinces in Brazil include one of the largest mafic-potassic provinces in the world (Alto Paranaíba Igneous Province, APIP), with the presence of mantle xenoliths enclosed in ultramafic rocks brought up by rapid ascension magmas (e.g., kimberlites, kamafugites). The occurrence of these rocks is an opportunity to directly study the SCLM, with implications for the geological models of tectonothermal evolution of the Brazilian Platform.

The Azimuth 125º Lineament (Bardet 1977; Figure 1) is a key area to understand the distribution of carbonatite and kimberlite-like rocks in Brazil. The WNW-ESE-trending zone contains Permian-Triassic to Late Cretaceous alkaline and mafic-potassic intrusions emplaced in distinct tectonic settings, including rocks from the Amazonian Craton, in Rondônia and Mato Grosso states and rocks from the São Francisco Craton and the Brasília Belt, in Minas Gerais State. These rocks are related to mineral deposits rich in phosphate, diamond, niobium, titanium and rare earth elements (e.g., Carvalho and Bressan 1981; Cordeiro et al. 2010, 2011). Despite the area's significance, publications about peridotitic, pyroxenitic and/or eclogitic mantle xenoliths are scarce, primarily those using modern analytical techniques. Compositional data coupled

ISSN: 2595-1939
https://doi.org/10.29396/jgsb.2022.v5.n3.2
Open access at jgsb.cprm.gov.br

with pressure and temperature calculations from garnet peridotite and eclogite samples from Rondônia and Mato Grosso states, are present in some unpublished academic thesis and dissertations (e.g., Costa 1996; Costa 2013; Weska and Svisero 2001; Nannini 2016; Cabral Neto et al. 2017a), whereas significant international publications are restricted to the study of diamonds derived from the lithospheric and sublithospheric mantle (e.g., Kaminsky et al. 2010; Pearson et al. 2014b; Hunt et al. 2009; Thomson et al. 2016; Borges et al. 2016; Rudloff-Grund et al. 2016; Navon et al. 2017). Mantle xenoliths hosted by kimberlites and kamafugites are otherwise more reported in papers from the APIP (Meyer and Svisero 1991; Leonardos et al. 1993; Carlson et al. 2007; Almeida et al. 2014; Nannini 2016; Fernandes et al. 2021). Overall, the geophysical, isotopic and microstructural data on peridotite samples provide evidence for the presence of remnants of an Archean cratonic root beneath the Brasília Belt in the region of the APIP (Carlson et al. 2007; Pinto 2009; Fernandes et al. 2021).

In order to provide a broader view regarding the nature of the SCLM beneath the Azimuth 125º Lineament, we present new data on the composition of (mantle) peridotite xenoliths enclosed in diamond-bearing kimberlites from Rondônia and Minas Gerais states in comparison with a comprehensive compilation of data from previous works. The peridotite samples are enclosed in Cosmos-1 and Carolina-1 kimberlites from Rondônia (Pimenta Bueno kimberlite field) and Canastra-1 kimberlite from APIP. We report mineral compositions of peridotite xenoliths from these kimberlite pipes, and derived *P-T* calculations for equilibrium mineral assemblages. An extended scope of this study is to compare the geothermal gradients between the two areas and discuss the implications for diamond genesis and the preservation of cratonic roots beneath the Azimuth 125º Lineament.

2. Analytical techniques

Mantle xenoliths enclosed in Cosmos-1 and Carolina-1 kimberlites were identified and collected from drill cores in the Geological Survey of Brazil facilities. The thin sections were described and selected for electron microprobe analyses based on the existence of well preserved mantle minerals (olivine, pyroxene and garnet). Major elements in minerals were analyzed with JEOL JXA-8200 and JEOL JXA-8230 electron microprobes at the CRTI (Federal University of Goiás) and São Paulo State University, respectively. Analyses were performed at 15 kV acceleration voltage and 20 nA beam current; beam diameter was normally 5 µm. The analyses performed at CRTI include the following standards: enstatite (Si), SiO_2 (Si), Al_2O_3 (Al), TiO_2 (Ti), olivine (Mg), jadeite (Na), orthoclase (K), diopside (Ca), Mn (Mn), Fe_3O_4 (Fe), olivine (Ni) and ZnO (Zn). The analyses performed at São Paulo State University include the standards: orthoclase (Si, K), wollastonite (Ca), anorthite (Al), albite (Na), olivine (Mg), ilmenite (Fe, Ti), rodonite (Mn), chromite (Cr), celestine (Zn) and NiO (Ni). Corrections were performed according to the ZAF method. The mineral structural formulas were calculated using Winpyrox (Yavuz 2013), Wingrt (Yavuz and Yildirim 2020), the spreadsheet of Locock (2008) and Minpet (Richard 1995). Temperature and pressure estimates were obtained using the spreadsheet PTEXCL (available at cms.eas.ualberta.ca/team-diamond/downloads/) and the software PTQuick (Simakov and Dolivo-Dobrovolsky 2009).

3. Geological Setting

The Azimuth 125º Lineament (Figure 1) is a zone that extends from the north to the southeast of Brazil that presents a concentration of carbonatite, kimberlite and kamafugite along with diamond occurrences. It was first described by Bardet (1977) as a zone of diamond occurrences from Minas Gerais to Rondônia states. However, the extension of the lineament is under debate, as some works do not consider that it extends from Mato Grosso to Rondônia states, based on the lack of aeromagnetic geophysical evidence in this area (Rocha 2013; Rocha et al. 2019), whereas other authors consider that it extends from Rondônia to Rio de Janeiro states (e.g., Gonzaga and Tompkins 1991; Zaffari et al. 2018). In fact, in Rondônia, there are three kimberlite fields (Pimenta Bueno, Ariquemes, Colorado D'Oeste) that have Permian-Carboniferous (Colorado D'Oeste, 268 ± 9 Ma, U-Pb perovskite; Felgate 2014) and Triassic aged rocks (Pimenta Bueno, 243.9 ± 2.4, Rb-Sr phlogopite; Felgate 2014), both cross-cut Paleozoic units from the Parecis Basin (e.g., Pimenta Bueno Graben; Quadros and Rizzotto 2007) and Paleo to Mesoproterozoic units of the southwestern portions of the Amazonian Craton (1.8-1.0 Ga; Tassinari and Macambira 1999). Petrological and geochronological data from these occurrences are scarce, especially for the Ariquemes kimberlite field, for which the ages of the intrusions are still unknown. Textural features of the lithotypes from the region are similar to those found in pipes from South Africa (Masun and Scott-Smith 2008).

The kimberlite pipes from the Mato Grosso state are grouped in the Juína, Paranatinga, Traíra and Jauru fields. The region has been responsible for significant diamond production since 1970 (Kaminski et al. 2010; Costa 2013; Nannini et al. 2017). The region of Juína presents a greater number of kimberlite occurrences, also cross-cutting the crystalline basement of the Amazonian Craton and units from the Parecis Basin (Kaminski et al. 2010). The kimberlites from Juína are younger (~91-95 Ma, U-Pb zircon; Heaman et al 1998; Kaminski et al 2010) than those from Paranatinga (126-120 Ma, U-Pb zircon; Heaman et al. 1998), and the kimberlite pipes comprise crater facies lithotypes, with pyroclastic and epiclastic rocks and diatreme facies breccias (Nannini et al. 2017).

The Minas Gerais and Goiás states present kimberlite pipes from the Alto Paranaíba Igneous Province (APIP; Gibson et al. 1995; Cabral Neto et al. 2017b), one of the largest mafic-potassic provinces in the world (>15000 km^3 in volume; Gibson et al. 1995). Despite the significant number of kimberlites in the area, only a few occurrences were subjected to petrological studies (Cabral Neto et al. 2017b). The region presents crater, diatreme and hypabyssal kimberlite pipes, with ages from 90 to 80 Ma, and lamproites, carbonatites and kamafugite lava flows (e.g., Mata da Corda Formation; Carlson et al. 1996). Lava flows also occur in the Goiás Alkaline Province to the northwest (e.g., Santo Antônio da Barra; 80-85 Ma Junqueira-Brod et al. 2002), together with subvolcanic and mafic-ultramafic alkaline complexes (e.g., Iporá; Junqueira-Brod et al. 2002). Many kimberlite pipes from the APIP occur in the Brasília Belt, surrounding the Paraná Basin and next to the western margin of the São Francisco Craton.

3.1. The Cosmos-1 and Carolina-1 kimberlites

The mantle xenoliths from Rondônia investigated in this work were sampled from the Cosmos-1 and Carolina

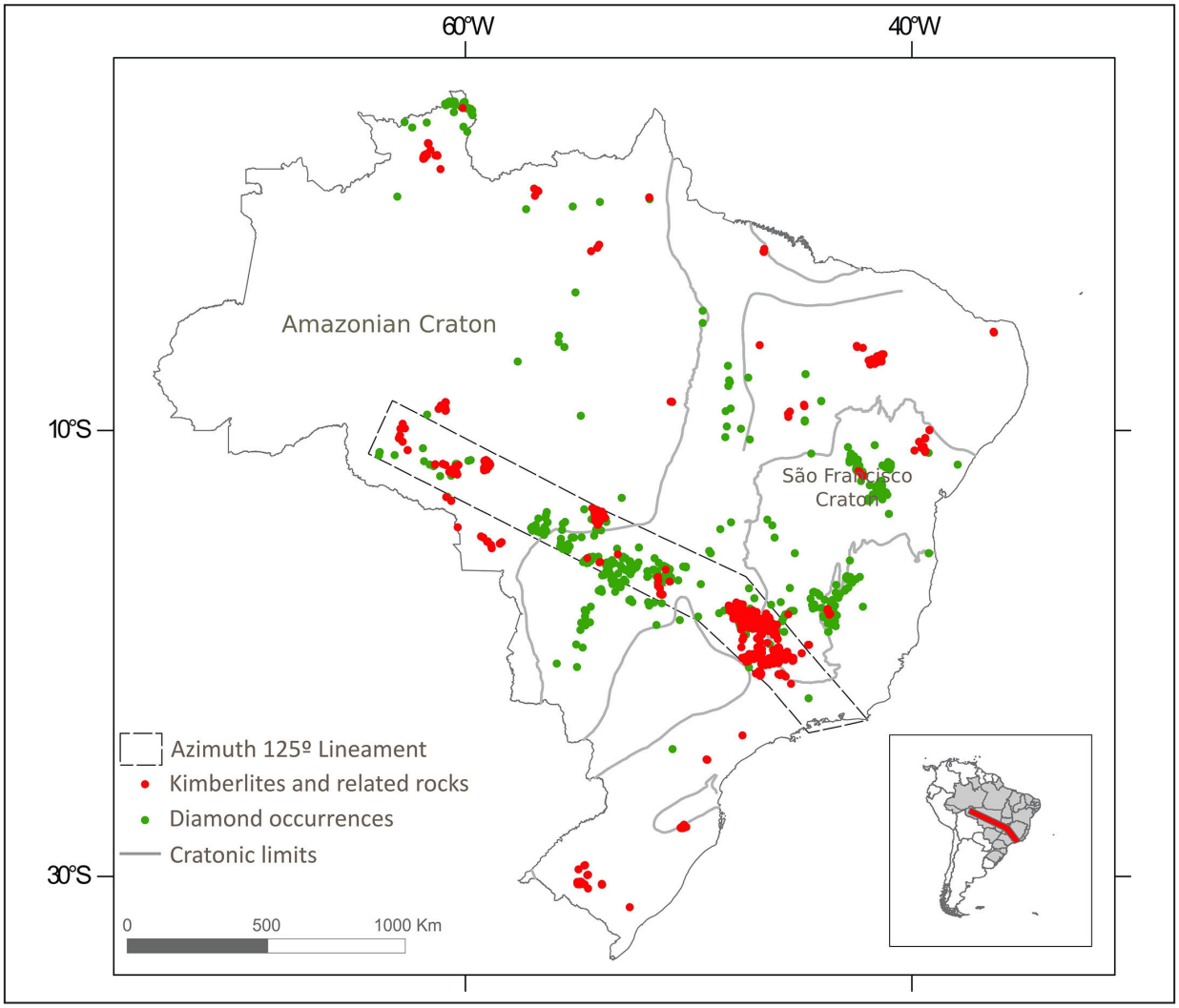

FIGURE 1 – Location of the Azimuth 125º Lineament area from Rondônia to Rio de Janeiro states (Gonzaga and Tompkins 1991) with the cratonic limits in the Brazilian territory (Cordani et al. 2016). The location of the kimberlites and diamond occurrences in Brazil is available at geoportal.cprm.gov.br/diamante.

kimberlites, both belonging to the Pimenta Bueno kimberlite field (Figure 2a). The area presents 54 known intrusions, located within and adjacent to the Pimenta Bueno Graben (Cabral Neto et al. 2017a). According to Masun and Scott Smith (2008), the pipes are similar to the kimberlites from South Africa.

The Cosmos-1 is located in the Cosmos-Pepper cluster and is cross-cutting Paleozoic units of the Pimenta Bueno Graben. The intrusion presents 2.3 ha and was the subject of a textural study by Masun and Scott Smith (2008). The authors described the presence of common mantle xenoliths together with olivine, ilmenite, peridotitic garnet and rare eclogitic garnet xenocrysts in Cosmos-1. A total of 117 diamonds (2.45 ct) were recovered from 62.2 tons of rocks from the intrusion (Cabral Neto et al. 2017a).

The Carolina-1 kimberlite is located in the Carolina cluster that comprises only two intrusions (Carolina-1 and Cometa-1) with diatreme and hypabyssal facies, respectively (Cabral Neto et al. 2017a). The intrusion presents 1.2 ha and is cross-cutting Mesoproterozoic units of the Amazonian Craton, next to the edge of the Pimenta Bueno Graben (Cabral Neto et al. 2017a; Figure 2a). The kimberlite age was determined at 232 ± 2.3 Ma based on Rb-Sr in phlogopite (Hunt et al. 2009). Hunt et al. (2009) described the Carolina kimberlite as an unconventional diamond deposit since the diamond potentially derives from an eclogitic source. Between 10000 to 12000 ct of diamonds were recovered from alluvial/colluvial deposits close to the intrusion (Maunula 2006).

3.2. The Canastra-1 Kimberlite

The mantle xenoliths from Minas Gerais investigated in this work are enclosed in the Canastra-1 kimberlite in the APIP (e.g., Gibson et al. 1995). There are 973 known kimberlite intrusions in Minas Gerais and adjacent areas that were grouped by Cabral Neto et al. (2017b) in 12 kimberlite fields. The Canastra-1 is located in the Serra da Canastra kimberlite field (Figure 2b) and presents 1.8 ha. The pipe cuts through greenschist facies metasedimentary rocks of the Canastra Group, Brasília Belt (Figure 2b). A K-Ar age of 120 Ma in phlogopite was obtained for the intrusion (Pereira and Fuck 2005). It is considered the first mineralized kimberlite from Brazil that is economically viable for exploitation from a primary source (Chaves et al. 2008a,b; Cabral Neto et al. 2017b). Microstructural and petrological data of peridotite mantle xenoliths were obtained by Costa (2008) and Fernandes et al. (2021).

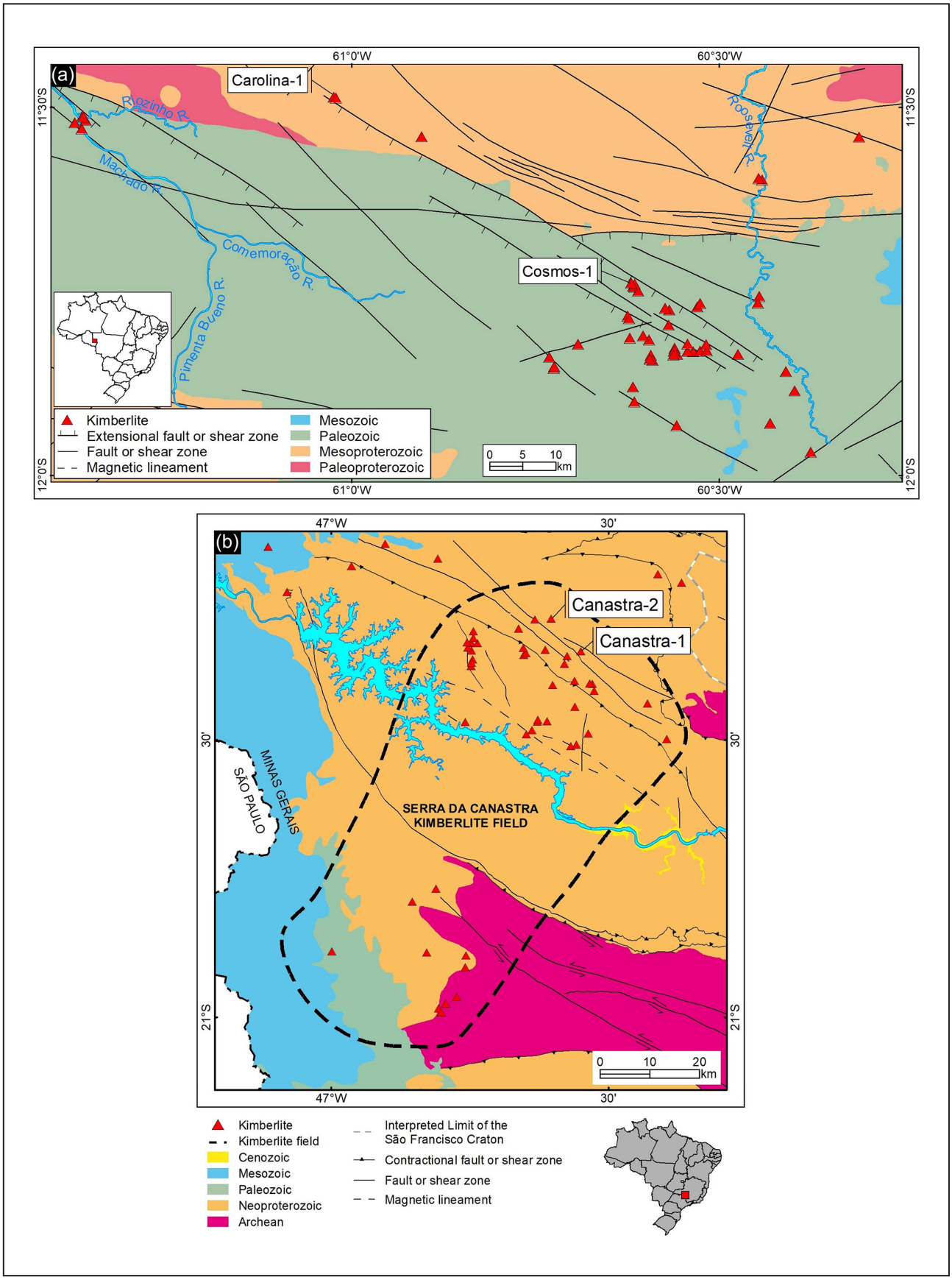

FIGURE 2 – (a) Geological map of the Pimenta Bueno kimberlite field in Rondônia, with the location of Cosmos-1 and Carolina-1 kimberlites; (b) Geological map of the Serra da Canastra kimberlite field in the APIP, with the location of Canastra-1 and 2 kimberlites. Adapted from Cabral Neto et al. (2017a).

4. Mantle xenoliths

The composition of the most preserved peridotite samples investigated in this work is plotted in the ternary diagram in Figure 3. The mineral proportions of representative thin sections are in Table 1. The Cosmos-1 kimberlite presents a fine-grained matrix where millimetre and centimetre-size xenoliths from the country rock are disposed together with millimetre and centimetre-size macrocrysts and xenocrysts of phlogopite, garnet, clinopyroxene, olivine pseudomorphs and ilmenite (Figure 4a). Partially and completely altered peridotite xenoliths also occur. The abundance of xenoliths from the country rock decreases with depth, while the occurrence of larger mantle xenoliths embedded in the kimberlite matrix are more frequent in the deeper parts of the drill cores. The mantle xenoliths are rounded, medium- to coarse-grained, up to 5 cm in diameter, composed of both serpentinised and well-preserved grains of 1-2 mm light-green clinopyroxene and 1-5 mm size lilac garnet (Figures 4b-c, 5a-b). The lack of other well preserved mineral phases in the investigated samples harmed the correct petrographic classification of the peridotites. In thin section, a reaction rim between the partially altered peridotite xenoliths and the host kimberlite is observed. Smaller clinopyroxene grains also occur included in garnet. Some samples present aggregates of clinopyroxene neoblasts (<0.1 mm) located along fractures and grain boundaries of deformed clinopyroxene grains with undulose extinction and deformation twins (Figure 5b-c). Kelyphitic rims composed of small grains of spinel and phlogopite surrounding garnet grains locally occur (Figure 5d).

The Carolina-1 kimberlite presents a fine-grained matrix and variable proportions of xenoliths of the country rock (e.g., amphibolite, gneiss) and millimetre to centimetre-size phlogopite and olivine macrocrysts, garnet xenocrysts and peridotite xenoliths (Figure 4d). The abundance of xenoliths from the country rock decreases with depth. Centimetre and decimetre-size rutile-bearing eclogite and clinopyroxene-phlogopite xenoliths also occur, but are not the focus of the present work. The peridotite xenoliths are rounded, up to 12 cm in diameter, with massive or foliated structures (Figures 4e-f). Some samples present a thick serpentinized rim with a well preserved core (Figure 4f). The olivine grains are better preserved in these samples, but partially serpentinized peridotite xenoliths only with pyroxene and garnet also occur. The most preserved peridotite samples are classified as dunites (Figure 3). Among these, one garnet-bearing dunite has a porphyroclastic texture (Figure 5e) in which large olivine grains are surrounded by an olivine neoblasts (<0.1 mm) matrix. Small pyroxene grains surrounded by olivine neoblasts occur in altered domains (Figure 5e).

The peridotite xenoliths enclosed in the Canastra-1 kimberlite are medium- to coarse-grained garnet harzburgite, garnet lherzolites and wehrlite with 7-13 cm wide in diameter (Figure 3, 4g-h). The samples are massive or foliated. The garnet harzburgite xenoliths show a protogranular-

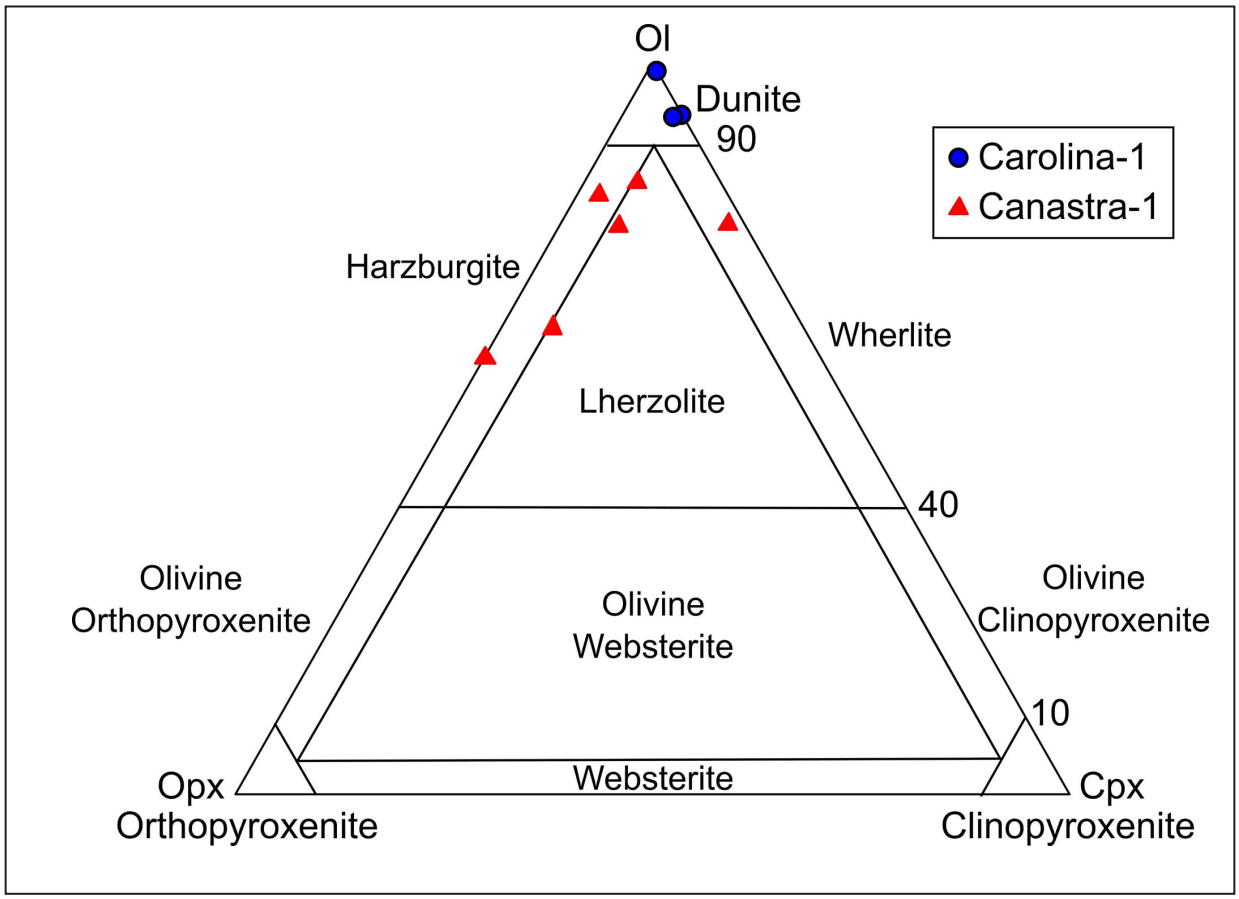

FIGURE 3 – Modal classification of the fresh peridotite xenoliths based on the proportions of olivine (Ol), orthopyroxene (Opx) and clinopyroxene (Cpx) (Streckeisen 1973).

porphyroclastic transitional texture and a porphyroclastic texture with ~65% vol.% of neoblasts. Anhedral 0.5-2 mm garnet grains present tiny spinel grains at the rims (Figure 6a). There are portions with concentration of olivine neoblasts (<0.1 mm) (Figure 6b). Up to 1.5 cm size olivine grains show undulose extinction and microfractures filled with serpentine. Small orthopyroxene neoblasts (<<0.1 mm) locally occur at grain boundaries of larger deformed orthopyroxene grains (2-10 mm). Garnet lherzolites show protogranular textures with lobated and straight contacts between the minerals. Reaction rim coronas composed of phlogopite and light-green clinopyroxene surrounding garnet are present in these samples (Figure 6c). Clinopyroxene can also occurs in reaction rims surrounding orthopyroxene and as anhedral grains of 1-3 mm. The wehrlite presents a porphyroclastic texture with olivine (6 mm) and light-green clinopyroxene porphyroclasts (2-6 mm) in a matrix with small olivine neoblasts and serpentine (Figure 6d). The olivine porphyroclasts show undulose extinction and deformation lamellaes. Small spinel grains included in clinopyroxene locally occur.

5. Electron microprobe data

5.1. Major element composition

Representative composition of the main minerals (olivine, orthopyroxene, clinopyroxene, spinel and garnet) are shown in tables 2-5. The mantle xenoliths enclosed in the Cosmos-1 kimberlite present only olivine pseudomorphs composed of serpentine and fine-grained micaceous material, so fresh olivine grains of the xenoliths from Rondônia were only analyzed in a porphyroclastic garnet dunite (VV-36) and a partially altered peridotite (VV-44) enclosed in Carolina-1 kimberlite. The olivine of the garnet dunite has high Mg# (100*Mg/Mg+Fe) (91.8-92.0) with no considerable variation from core to rim or between neoblasts and porphyroclasts (Table 2). NiO ranges from 0.36 to 0.41 wt%. The partially altered peridotite presents olivine grains with higher concentration in FeO (11.7-11.9 wt%) and NiO contents from 0.35 to 0.4 wt%.

The olivine of the peridotites enclosed in the Canastra-1 kimberlite presents variable Mg# values, with FeO ranging from 6 to 9.8 wt%, while NiO contents are from 0.3 to 0.5 wt%. The olivine of the harzburgite xenolith presents higher Mg# values with a narrow range (93.6-93.9), with the lowest FeO content (6-6.3 wt%), while the olivine from the lherzolite VV-33 presents Mg# from 91.9 to 92.3, with FeO from 7.5 to 7.9 wt%. The lherzolite VV-31 presents olivine grains with distinct Mg# (89.9-93.4) with rims with slightly lower Mg# and higher FeO (7.9-9.7wt%). The olivine of the wehrlite shows Mg# from 92.0 to 92.4 and FeO from 7.5 to 7.9 wt%.

The garnet dunite (VV-36) enclosed in Carolina-1 kimberlite is the only examined sample from Rondônia that presents orthopyroxene relics. In this case, the grains present Mg# from 90.5 to 91.7 and 0.1 wt% of TiO_2. The harzburgite (VV-32) of the Canastra-1 kimberlite presents higher Mg# (93.8-94.7), while the lherzolites show grains with lower Mg# from 91.2 to 92.8 (VV-33) and 92.1 to 94.4 (VV-31) (figures 7a and 8a). The grains of the sample VV-31 show a wide range of the Mg# from 90.8 (rim) to 94.4 (points both in core and rim; Figure 8a).

The clinopyroxene composition is shown in figures 7b-e, 8b and 9. All the grains of the xenoliths from Rondônia are Ca-Mg-Fe clinopyroxenes (augite and diopside) with Mg# ranging from 81.4 (rim) to 93.3 in partially altered peridotites, while the grains in garnet dunite show Mg# from 88.8 to 92.2. Most of the grains present Cr# (Cr/Cr+Al) between 0.2 and 0.3, except for the partially altered peridotite VV-44, which presents several points with higher Cr# (>0.7). The clinopyroxene of the Canastra-1 samples are diopside and augite grains with Mg# from 90.8 to 92.8 in the wehrlite and from 88.4 (rim) to 94.3 in the lherzolites. In general, the clinopyroxene of the lherzolite VV-34 shows higher Na apfu and some grains located in reaction rim coronas surrounding garnet can be classified as omphacite (figures 7c and 8b). The grains present Cr# from 0.1 (lherzolite) to 0.6 (wehrlite). The composition of the clinopyroxene from both localities (Rondônia and Minas Gerais) is predominantly in the on craton garnet peridotite field of Figure 9a-b (Ramsay 1992).

The investigated garnet grains of the samples from Rondônia were sampled from peridotite xenoliths and as xenocrysts surrounded by the kimberlitic matrix. The composition of the garnet is dominated by pyrope (53-76 mol%), 2-20 mol% almandine and 3-21 mol% uvarovite (Figure

TABLE 1. Mineral proportions of representative thin sections of peridotite xenoliths.

Sample	Lithotype	Ol	Cpx	Opx	Grt	Sp	Phl	Opc	Chl	Alt. (Srp)	Cb	Tlc	Host rock	Matrix
VV-1A	Partially altered peridotite	-	10	-	25	-	2	-	tr	63	-	-	-	-
VV-2	Partially altered peridotite	-	4	-	5	-	2	2	tr	84	-	3	-	-
VV-3	Partially altered peridotite	-	7	-	6	-	-	2	-	82	1	2	-	-
VV-4	Partially altered peridotite	-	7	-	6	-	-	2	-	74	8	3	-	-
VV-5B*	Partially altered peridotite	-	Tr	-	4	-	1	9	tr	25	-	6	20	35
VV-27	Partially altered peridotite	-	30	-	-	-	-	3	-	67	-	-	-	-
VV-29	Wehrlite	78	20	2	-	tr	-	-	-	-	-	-	-	-
VV-30	Grt harzburgite	75	2	14	6	tr	3	tr	-	-	-	-	-	-
VV-31	Lherzolite	53	5	25	7	-	7	3	-	-	-	-	-	-
VV-32	Harzburgite	52		35	10	3	-	-	-	-	-	-	-	-
VV-33	Lherzolite	67	5	8	20	-	-	-	-	-	-	-	-	-
VV-34	Lherzolite	66	6	13	10	tr	5	-	-	-	-	-	-	-
VV-36	Grt dunite	77	5	1	3	-	2	-	-	-	-	-	-	-
VV-44	Partially altered peridotite	-	6	-	5	-	tr	-	1	80	-	-	-	-
VV-52	Partially altered peridotite	Tr	1	-	5	-	1	-	tr	90	-	-	-	-

*Thin section of the Cosmos-1 kimberlite with garnet xenocrysts locally with inclusion of clinopyroxene.
Ol – olivine, Cpx – clinopyroxene, Opx – orthopyroxene, Grt – garnet, Sp – spinel, Phl – phlogopite, Opc – opaque minerals, Chl – chlorite, Alt. - alteration, Srp – serpentine, Cb – carbonate, Tlc – talc, tr- trace, Host rock – xenoliths of the host rock, Matrix – fine-grained matrix.

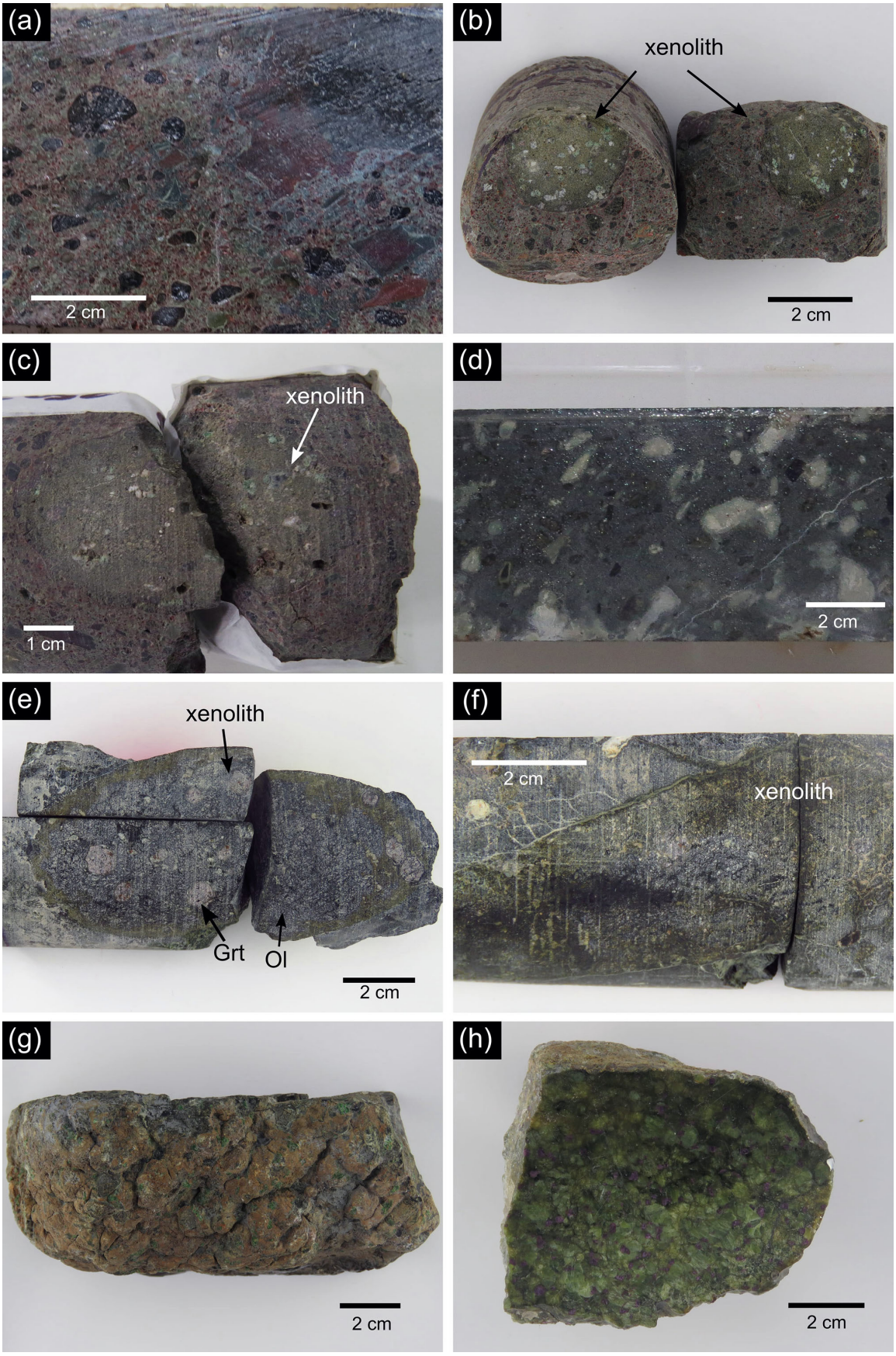

FIGURE 4 – (a) Drill core of the Cosmos-1 kimberlite showing a fine-grained matrix with xenoliths, xenocrysts and macrocrysts; (b) and (c) Partially altered peridotite xenoliths found in drill cores of the Cosmos-1 kimberlite; (d) Drill core of the Carolina-1 kimberlite showing a fine-grained matrix with xenoliths, xenocrysts and macrocrysts; (e) and (f) Peridotite xenoliths with serpentinized rims found in drill cores of the Carolina-1 kimberlite; (g) and (h) Peridotite xenoliths of the Canastra-1 kimberlite.

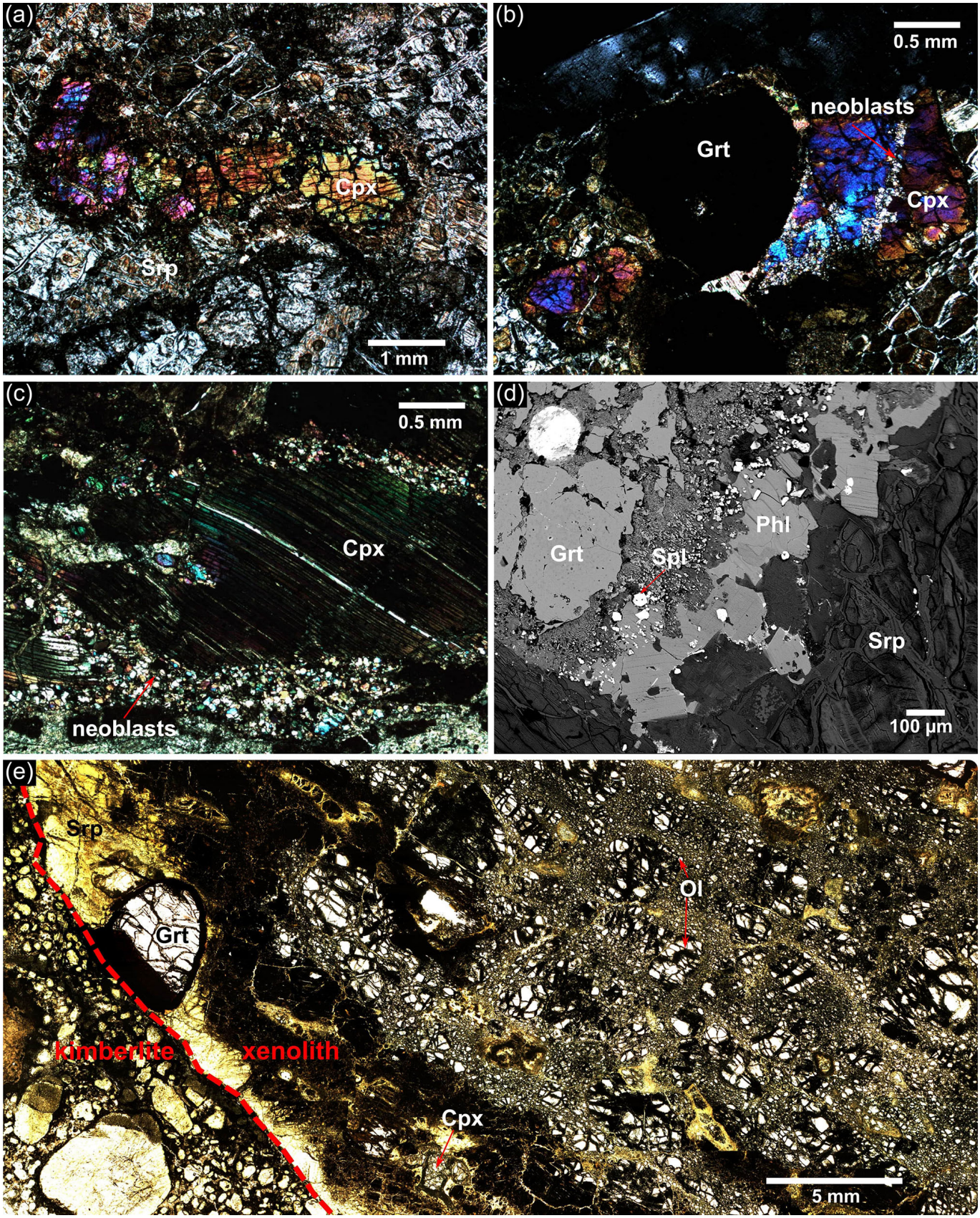

FIGURE 5 – Photomicrographs of peridotite xenoliths enclosed in kimberlites from Rondônia. (a) Preserved clinopyroxene (Cpx) grains surrounded by serpentine (Srp) in a partially altered peridotite; (b) Clinopyroxene neoblasts located in microfractures of larger clinopyroxene grains; (c) Small clinopyroxene neoblasts located along fractures and limits of deformed clinopyroxene grains; (d) Kelyphitic rim with spinel (Spl) and phlogopite (Phl) surrounding garnet (Grt); (e) Thin section of the porphyroclastic texture of a garnet dunite with the location of garnet, olivine (Ol) and clinopyroxene.

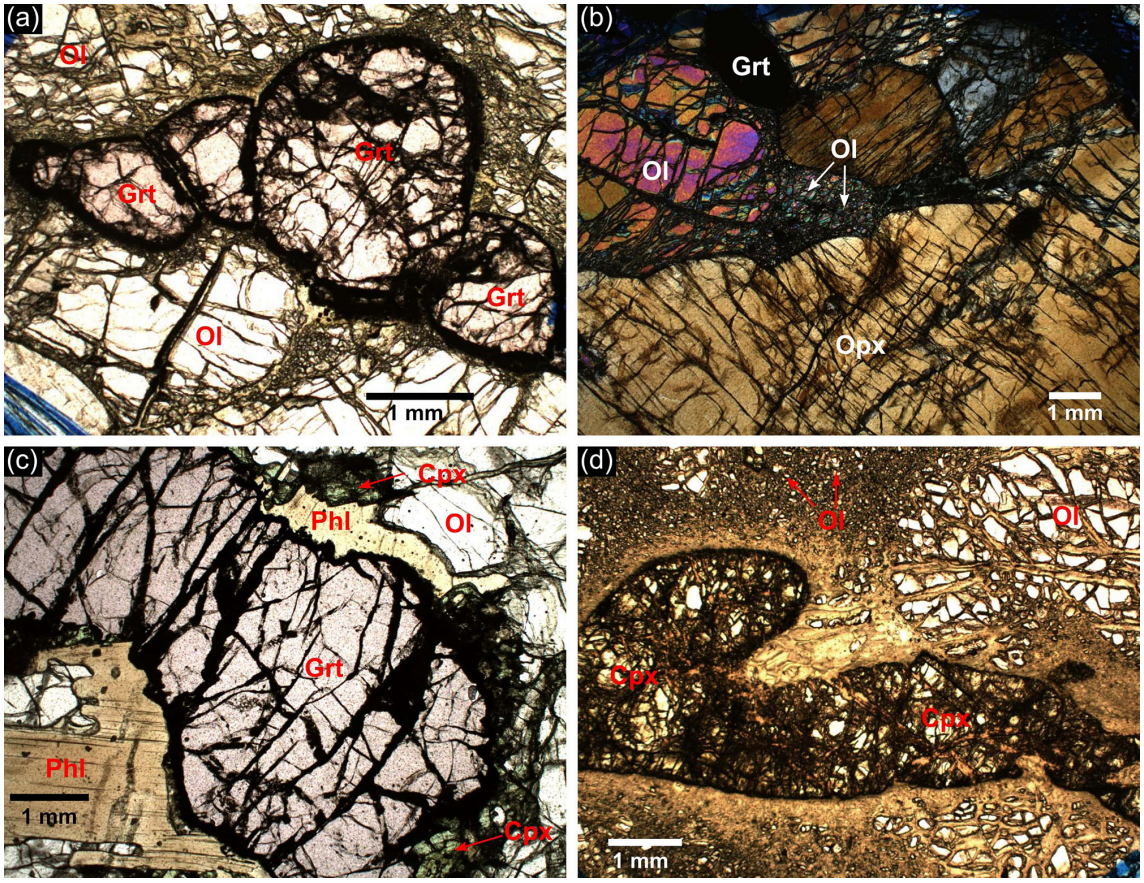

FIGURE 6 – Photomicrographs of peridotite xenoliths enclosed in the Canastra-1 kimberlite. (a) Garnet (Grt) grains in garnet harzburgite; (b) Olivine (Ol) neoblasts located in grain boundaries of garnet harzburgite; (c) Phlogopite (Phl) and clinopyroxene (Cpx) in coronas surrounding garnet in garnet lherzolite; (d) Olivine and clinopyroxene porphyroclasts surrounded by neoblasts.

TABLE 2. Representative composition of olivine of the peridotite xenoliths enclosed in the Carolina-1 (VV-36, VV-44) and Canastra-1 (VV-29, VV-31, VV-32, VV-33) kimberlites. Structural formulas are calculated on the basis of 4 oxygens.

Sample	VV36	VV36	VV36	VV44	VV44	VV29	VV29	VV32	VV32	VV32	VV33	VV33	VV31	VV31
Location	core	rim	int	core	rim	rim	core	core	rim	int	rim	int	rim	core
lithotype	dun	dun	dun	alt	alt	wehr	wehr	harz	harz	harz	lherz	lherz	lherz	lherz
SiO_2	41.66	41.11	41.53	40.05	39.84	41.35	41.18	41.59	41.20	41.34	41.17	40.66	40.74	41.32
Al_2O_3	0.03	0.01	0.00		0.06	0.01	0.01			0.01	0.02	0.03	0.03	0.04
Na_2O	0.04	0.02	0.00	0.00	0.03	0.01	0.01	0.00		0.03	0.01	0.06	0.03	0.02
MgO	49.47	49.25	49.72	47.26	46.99	51.33	51.06	51.68	51.60	51.44	50.53	50.19	49.15	50.83
CaO	0.04	0.04	0.04	0.03	0.04	0.02	0.03		0.01	0.02	0.02	0.13	0.07	0.05
TiO_2	0.03	0.03		0.01	0.00	0.01	0.02					0.02		0.03
Cr_2O_3	0.02	0.03	0.03	0.01	0.01	0.03	0.03	0.01	0.00	0.03	0.00	0.01	0.08	0.04
FeO	7.92	7.74	7.79	11.71	11.81	7.68	7.64	6.08	6.15	6.00	7.62	7.81	9.47	7.75
MnO	0.11	0.07	0.10	0.09	0.10	0.11	0.12	0.07	0.07	0.07	0.07	0.07	0.10	0.11
NiO	0.36	0.39	0.37	0.35	0.40	0.33	0.32	0.41	0.46	0.43	0.40	0.38	0.32	0.40
Total	99.68	98.69	99.58	99.51	99.28	100.88	100.42	99.84	99.49	99.37	99.84	99.36	99.99	100.59
Si	1.014	1.011	1.012	0.996	0.995	0.996	0.996	1.004	0.999	1.003	1.001	0.996	0.998	0.998
Al	0.001	0.000	0.000	0.000	0.002	0.000	0.000	0.000	0.000	0.000	0.001	0.001	0.001	0.001
Ti	0.001	0.001	0.000	0.000	0.000	0.000	0.000	0.000	0.000	0.000	0.000	0.000	0.000	0.001
Fe^2	0.161	0.159	0.159	0.244	0.247	0.155	0.155	0.123	0.125	0.122	0.155	0.160	0.194	0.157
Mn	0.002	0.001	0.002	0.002	0.002	0.002	0.002	0.001	0.001	0.001	0.001	0.001	0.002	0.002
Mg	1.796	1.806	1.806	1.753	1.749	1.843	1.841	1.860	1.866	1.860	1.832	1.832	1.795	1.831
Ca	0.001	0.001	0.001	0.001	0.001	0.001	0.001	0.000	0.000	0.001	0.001	0.003	0.002	0.001
Na	0.002	0.001	0.000	0.000	0.001	0.000	0.000	0.000	0.000	0.001	0.000	0.003	0.001	0.001
Ni	0.007	0.008	0.007	0.007	0.008	0.006	0.006	0.008	0.009	0.008	0.008	0.007	0.006	0.008
Cations	2.985	2.988	2.987	3.003	3.005	3.003	3.001	2.996	3.000	2.996	2.999	3.003	2.999	3.000
Fe#	8.2	8.1	8.1	12.2	12.4	7.8	7.8	6.2	6.3	6.2	7.8	8.0	9.8	7.9
Mg#	91.8	91.9	91.9	87.8	87.6	92.2	92.2	93.8	93.7	93.8	92.2	92.0	90.2	92.1

int – between core and rim; dun – dunite; alt – partially altered peridotite; wehr – wehrlite; harz – harzburgite; lherz – lherzolite.

TABLE 3. Representative composition of orthopyroxene of the peridotite xenoliths enclosed in the Carolina-1 (VV-36) and Canastra-1 (VV-31, VV-32, VV-33, VV-34) kimberlites. Structural formulas are calculated on the basis of 6 oxygens.

Sample	VV-36	VV-36	VV-31	VV-31	VV-32	VV-32	VV-32	VV-34	VV-34	VV-33	VV-33
Location	int	int	rim	core	core	int	rim	int	int	int	int
Lithotype	dun	dun	lherz	lherz	harz	harz	harz	lherz	lherz	lherz	lherz
SiO_2	58.18	57.56	57.90	58.55	58.25	58.06	58.28	58.84	58.61	57.65	58.20
TiO_2	0.11	0.12	0.00	0.00	0.00	0.00	0.00	0.01	0.00	0.00	0.00
Al_2O_3	0.71	0.67	0.76	0.72	0.88	0.83	0.82	0.81	0.81	0.77	0.71
Cr_2O_3	0.23	0.22	0.36	0.35	0.35	0.37	0.37	0.39	0.39	0.22	0.27
FeO	4.71	4.60	3.90	3.95	3.77	3.80	3.63	4.00	3.98	4.97	4.87
MnO	0.10	0.09	0.09	0.12	0.07	0.08	0.07	0.12	0.09	0.11	0.08
NiO	0.12	0.09	0.10	0.11	0.10	0.09	0.09	0.12	0.11	0.08	0.07
MgO	34.94	34.24	36.60	36.63	36.39	36.50	36.54	35.99	36.16	35.48	35.92
CaO	0.53	0.68	0.37	0.36	0.31	0.29	0.28	0.43	0.39	0.26	0.20
Na_2O	0.18	0.17	0.08	0.09	0.11	0.12	0.15	0.09	0.09	0.07	0.03
K_2O	0.01	0.09	0.00	0.00	0.01	0.00	0.00	0.01	0.00	0.00	0.01
Total	99.81	98.54	100.16	100.87	100.22	100.13	100.23	100.81	100.65	99.60	100.36
Si (T)	1.986	1.988	1.969	1.979	1.981	1.975	1.980	1.982	1.982	1.982	1.983
Al (T)	0.014	0.012	0.030	0.021	0.020	0.025	0.021	0.018	0.018	0.018	0.017
Fe^{3+} (T)	0.000	0.000	0.001	0.000	0.000	0.000	0.000	0.000	0.000	0.000	0.000
Total (T)	2.000	2.000	2.000	2.000	2.000	2.000	2.000	2.000	2.000	2.000	2.000
Al (M1)	0.014	0.015	0.000	0.008	0.016	0.008	0.013	0.014	0.014	0.013	0.012
Fe^{3+} (M1)	0.000	0.000	0.027	0.009	0.002	0.015	0.008	0.000	0.000	0.004	0.000
Ti (M1)	0.003	0.003	0.000	0.000	0.000	0.000	0.000	0.000	0.000	0.000	0.000
Cr (M1)	0.006	0.006	0.010	0.009	0.009	0.010	0.010	0.010	0.010	0.006	0.007
Ni (M1)	0.003	0.003	0.003	0.003	0.003	0.003	0.003	0.003	0.003	0.002	0.002
Mg (M1)	0.974	0.973	0.961	0.971	0.971	0.965	0.967	0.972	0.973	0.975	0.979
Fe^{2+} (M1)	0.000	0.000	0.000	0.000	0.000	0.000	0.000	0.000	0.000	0.000	0.000
Mn (M1)	0.000	0.000	0.000	0.000	0.000	0.000	0.000	0.000	0.000	0.000	0.000
Total (M1)	1.000	1.000	1.000	1.000	1.000	1.000	1.000	1.000	1.000	1.000	1.000
Mg (M2)	0.805	0.790	0.895	0.875	0.874	0.886	0.883	0.835	0.850	0.843	0.846
Fe^{2+} (M2)	0.161	0.166	0.084	0.103	0.105	0.093	0.095	0.140	0.127	0.139	0.142
Mn (M2)	0.003	0.003	0.003	0.003	0.002	0.002	0.002	0.003	0.003	0.003	0.002
Ca (M2)	0.019	0.025	0.013	0.013	0.011	0.011	0.010	0.015	0.014	0.010	0.007
Na (M2)	0.012	0.012	0.006	0.006	0.007	0.008	0.010	0.006	0.006	0.005	0.002
K (M2)	0.000	0.004	0.000	0.000	0.000	0.000	0.000	0.001	0.000	0.000	0.000
Total (M2)	1.000	1.000	1.000	1.000	1.000	1.000	1.000	1.000	1.000	1.000	1.000
Wo	1.0	1.3	0.7	0.7	0.6	0.5	0.5	0.8	0.7	0.5	0.4
En	90.8	90.2	95.0	94.1	94.1	94.7	94.6	92.1	92.8	92.4	92.4
Fs	8.2	8.5	4.3	5.2	5.4	4.8	4.9	7.1	6.5	7.1	7.2
Mg#	91.7	91.4	94.4	94.3	94.5	94.5	94.7	92.8	93.5	92.7	92.8

int – between core and rim; dun – dunite; alt – partially altered peridotite; wehr – wehrlite; harz – harzburgite; lherz – lherzolite.

Table 4. Representative composition of clinopyroxene of the peridotite xenoliths enclosed in the Cosmos-1 (VV-2, VV-3, VV-3, VV-4, VV-5b), Carolina-1 (VV-36, VV-44) and Canastra-1 (VV-29, VV-31, VV-33, VV-34) kimberlites. Structural formulas are calculated on the basis of 6 oxygens.

Sample	VV-02	VV-03	VV-03	VV-04	VV-05b	VV-36	VV-44	VV-29	VV-29	VV-31	VV-31	VV-33	VV-34	VV-34
Location	core	rim	core	core	core	int	core	rim	core	core	rim	core	rim	int
Lithotype	alt	alt	alt	alt	incl grt	dun	alt	wehr	wehr	lherz	lherz	lherz	lherz	lherz
SiO_2	53.90	54.55	54.92	54.69	54.71	55.04	54.22	55.36	55.33	54.06	54.39	55.14	55.80	55.82
TiO_2	0.08	0.31	0.31	0.33	0.24	0.30	0.12	0.25	0.25	1.00	0.65	0.00	0.13	0.09
Al_2O_3	1.85	1.95	1.93	1.97	2.57	2.44	1.17	1.74	1.74	1.17	0.82	2.08	3.31	2.49
Cr_2O_3	1.19	0.90	0.90	0.73	0.81	1.78	0.68	2.65	2.71	1.42	1.34	1.48	2.60	2.34
FeO	2.09	3.49	3.57	3.57	4.06	2.55	3.53	2.31	2.42	3.73	3.42	1.76	2.11	2.12
MnO	0.11	0.11	0.10	0.07	0.06	0.10	0.08	0.08	0.10	0.12	0.12	0.05	0.05	0.07
NiO	0.06	0.07	0.08	0.07	0.08	0.05	0.05	0.05	0.06	0.01	0.00	0.05	0.04	0.03
MgO	16.36	17.81	17.87	17.89	18.17	16.38	17.19	16.55	16.54	18.27	18.24	16.33	15.27	15.80
CaO	23.27	19.32	19.36	19.50	17.17	18.59	20.96	18.56	18.66	19.28	19.55	21.49	17.90	18.96
Na_2O	1.14	1.34	1.26	1.24	1.57	2.28	1.07	2.36	2.21	1.19	1.16	1.58	3.02	2.48
K_2O	0.01	0.03	0.03	0.04	0.03	0.03	0.02	0.02	0.02	0.00	0.00	0.01	0.01	0.00
Total	100.06	99.88	100.31	100.09	99.48	99.53	99.09	99.91	100.03	100.24	99.68	99.96	100.24	100.20
Si (T)	1.951	1.970	1.977	1.972	1.978	1.991	1.981	1.997	1.996	1.953	1.973	1.990	1.995	1.998
Al (T)	0.049	0.030	0.023	0.028	0.022	0.009	0.019	0.003	0.005	0.047	0.027	0.010	0.005	0.002
Fe^{3+} (T)	0.000	0.000	0.000	0.000	0.000	0.000	0.000	0.000	0.000	0.000	0.000	0.000	0.000	0.000
Total (T)	2.000	2.000	2.000	2.000	2.000	2.000	2.000	2.000	2.000	2.000	2.000	2.000	2.000	2.000
Al (M1)	0.030	0.053	0.059	0.055	0.088	0.095	0.032	0.071	0.070	0.003	0.009	0.078	0.134	0.103
Fe^{3+} (M1)	0.061	0.029	0.011	0.023	0.009	0.009	0.038	0.009	0.000	0.032	0.026	0.000	0.000	0.000
Ti (M1)	0.002	0.009	0.008	0.009	0.007	0.008	0.003	0.007	0.007	0.027	0.018	0.000	0.004	0.002
Cr (M1)	0.034	0.026	0.026	0.021	0.023	0.051	0.020	0.076	0.077	0.041	0.038	0.042	0.074	0.066
Ni (M1)	0.002	0.002	0.002	0.002	0.002	0.001	0.001	0.002	0.002	0.000	0.000	0.001	0.001	0.001
Mg (M1)	0.872	0.882	0.894	0.890	0.871	0.836	0.906	0.836	0.845	0.897	0.910	0.878	0.788	0.827
Fe^{2+} (M1)	0.000	0.000	0.000	0.000	0.000	0.000	0.000	0.000	0.000	0.000	0.000	0.000	0.000	0.000
Mn (M1)	0.000	0.000	0.000	0.000	0.000	0.000	0.000	0.000	0.000	0.000	0.000	0.000	0.000	0.000
Total (M1)	1.000	1.000	1.000	1.000	1.000	1.000	1.000	1.000	1.000	1.000	1.000	1.000	1.000	1.000
Mg (M2)	0.011	0.078	0.065	0.071	0.108	0.047	0.030	0.054	0.045	0.087	0.077	0.001	0.026	0.016
Fe^{2+} (M2)	0.003	0.076	0.096	0.085	0.114	0.068	0.070	0.061	0.076	0.080	0.078	0.056	0.077	0.082
Mn (M2)	0.004	0.003	0.003	0.002	0.002	0.003	0.003	0.002	0.003	0.004	0.004	0.002	0.002	0.002
Ca (M2)	0.902	0.748	0.747	0.753	0.665	0.721	0.821	0.717	0.721	0.746	0.760	0.831	0.686	0.727
Na (M2)	0.080	0.094	0.088	0.087	0.110	0.160	0.076	0.165	0.155	0.083	0.081	0.110	0.209	0.172
K (M2)	0.000	0.001	0.001	0.002	0.001	0.001	0.001	0.001	0.001	0.000	0.000	0.000	0.000	0.000
Total (M2)	1.000	1.000	1.000	1.000	1.000	1.000	1.000	1.000	1.000	1.000	1.000	1.000	1.000	1.000
Wo	50.5	41.9	41.4	41.9	37.8	43.1	44.9	43.0	42.8	41.2	41.7	47.1	43.5	44.0
En	49.4	53.8	53.2	53.4	55.7	52.8	51.3	53.4	52.7	54.4	54.1	49.8	51.6	51.0
Fs	0.2	4.3	5.3	4.7	6.5	4.1	3.8	3.6	4.5	4.4	4.3	3.2	4.9	5.0
Q	1.8	1.8	1.8	1.8	1.8	1.7	1.8	1.7	1.7	1.8	1.8	1.8	1.6	1.7
J	0.2	0.2	0.2	0.2	0.2	0.3	0.2	0.3	0.3	0.2	0.2	0.2	0.4	0.3
Mg#	93.3	90.1	89.9	89.9	88.9	92.0	89.7	92.7	92.2	89.7	90.5	94.0	91.4	91.1
Cr#	0.30	0.24	0.24	0.19	0.17	0.33	0.28	0.50	0.51	0.45	0.52	0.32	0.35	0.39

int – between core and rim; dun – dunite; alt – partially altered peridotite; wehr – wehrlite; incl grt – inclusion in garnet; lherz – lherzolite.

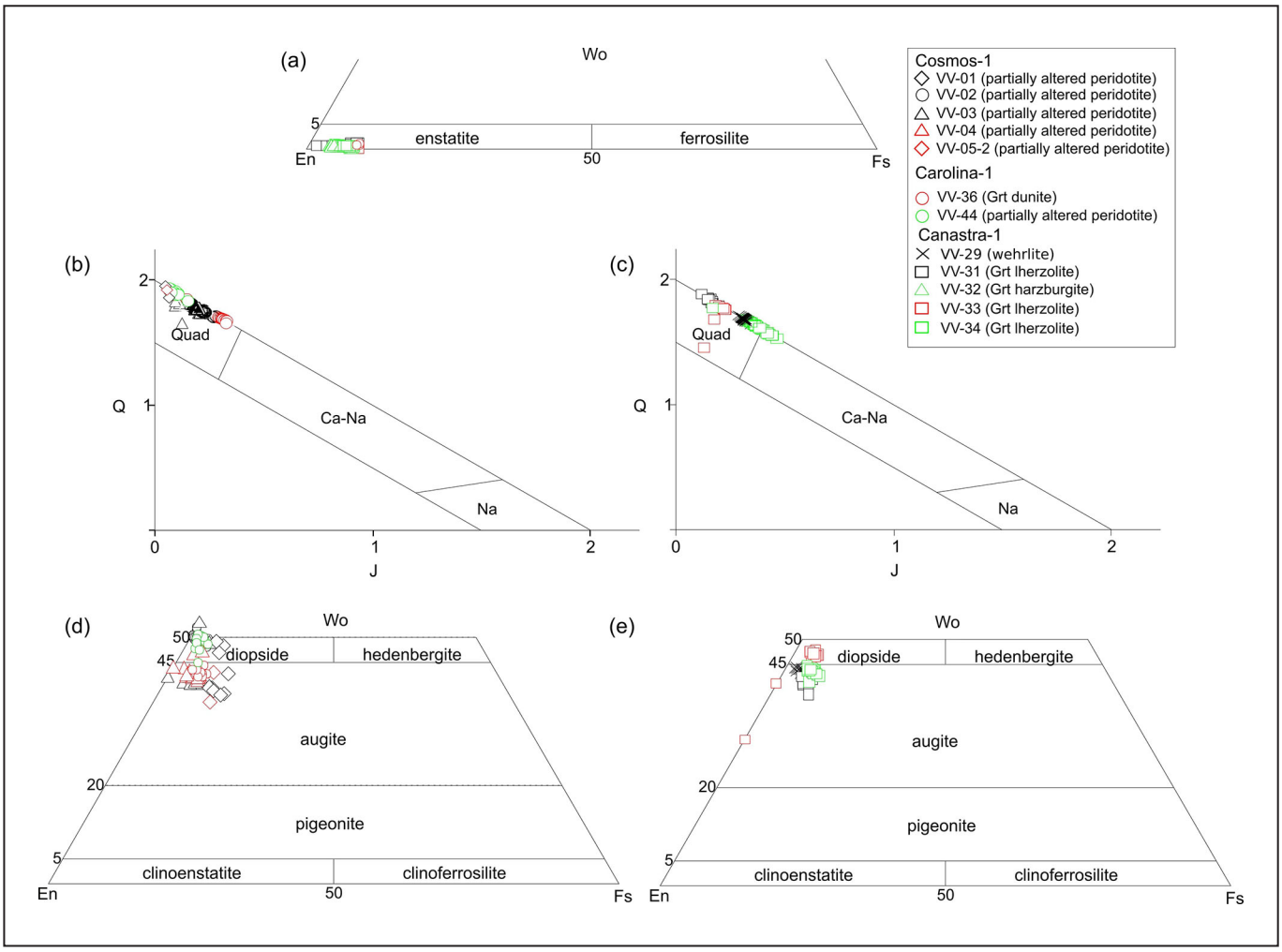

FIGURE 7 – (a) Diagram with the classification of the orthopyroxene grains; (b) Classification of the clinopyroxene grains of the Rondônia mantle xenoliths in the Q-J diagram of Morimoto (1988); (c) Classification of the clinopyroxene grains of the peridotite xenoliths enclosed in the Canastra-1 kimberlite in the Q-J diagram of Morimoto (1988); (d) Classification of the Ca-Mg-Fe clinopyroxene from Rondônia in the Morimoto diagram; (e) Classification of the Ca-Mg-Fe clinopyroxenes of the xenoliths from the Canastra-1 kimberlite.

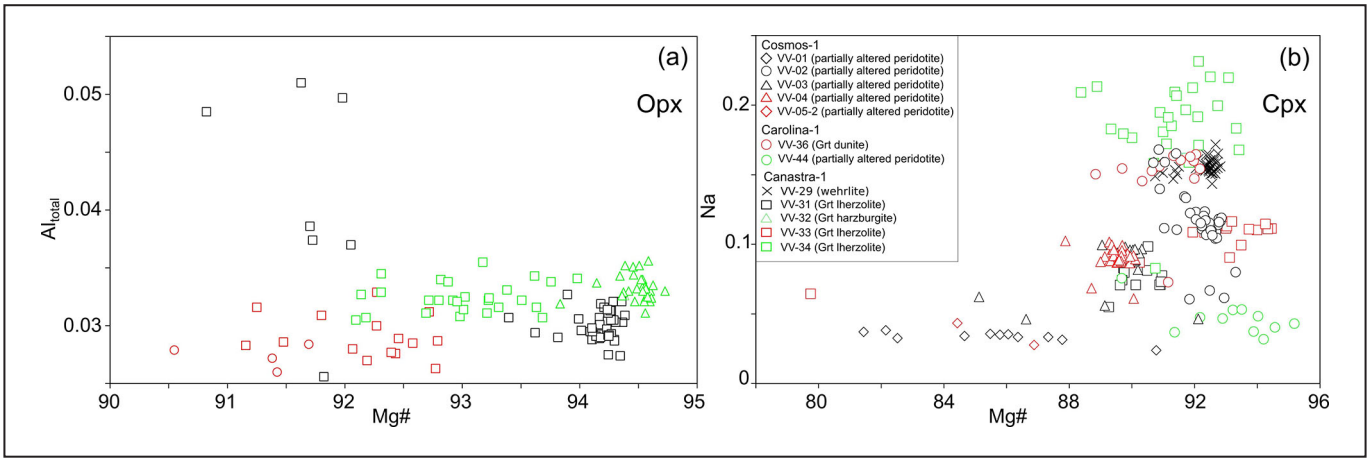

FIGURE 8 – (a) Mg# vs. Altotal and (b) Mg# vs. Na of orthopyroxene (Opx) and clinopyroxene (Cpx) grains, respectively.

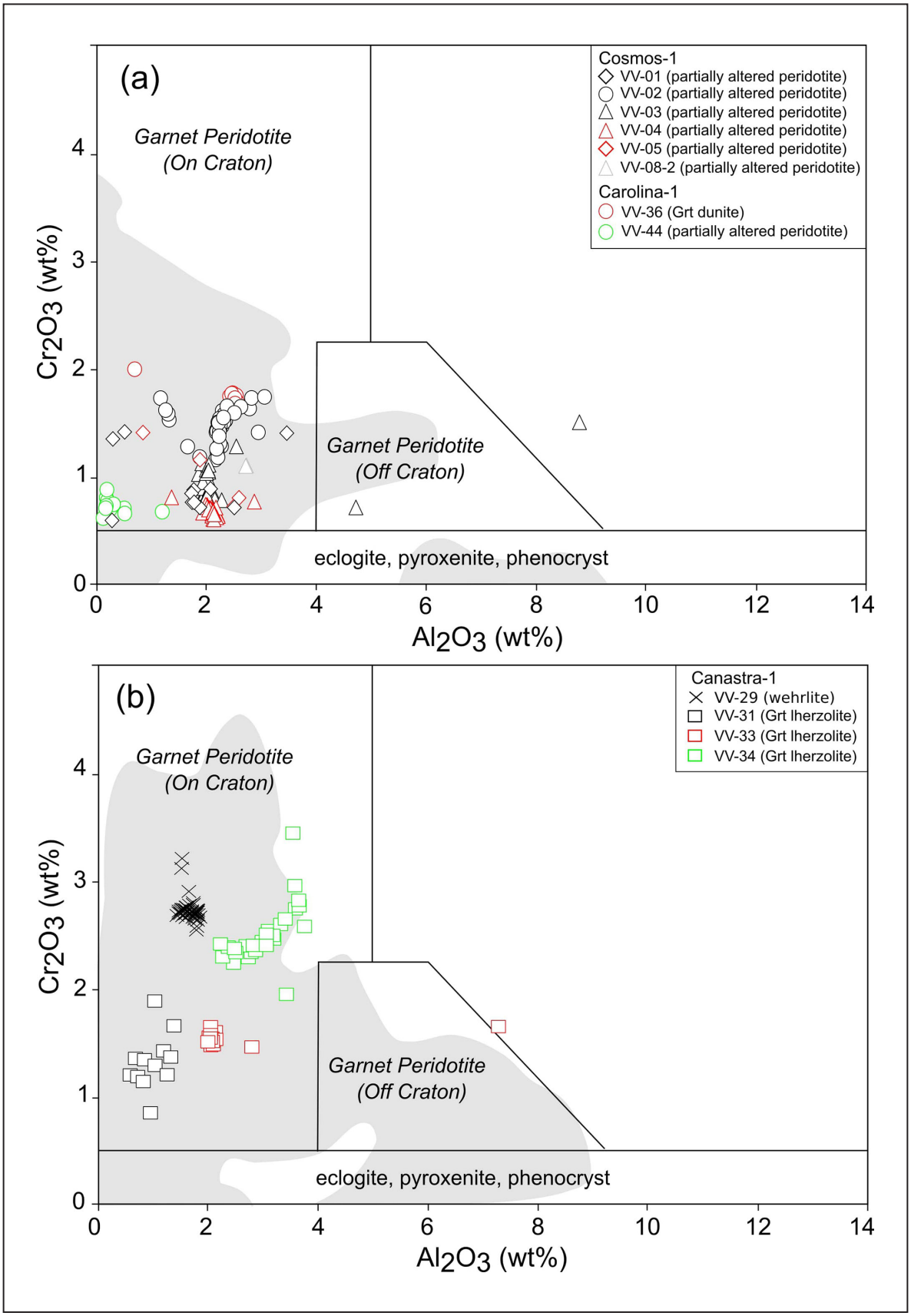

FIGURE 9 – Clinopyroxene Al_2O_3 vs Cr_2O_3 (wt%) classification diagram of Ramsay (1992) with the composition of the grains of Cosmos-1 and Carolina-1 samples in (a) and of the Canastra-1 samples in (b). The grey areas in (a) and (b) represent the composition of the clinopyroxene of mantle xenoliths and concentrates of the kimberlites from Rondônia (196 analyses) and APIP (1322 analyses), respectively, from previous works. Data compilation from: Costa (1996), Carvalho (1997), Zolinger (2005), Chaves (2008a), Costa (2008), Silva (2008), Melluso et al. (2008), Almeida (2009), Chaves et al. (2009), Thomaz (2009), Hunt et al. (2009), Nannini (2011), Andrade (2012), Guarino et al. (2013), Nannini (2016) and Gervasoni et al. (2022).

TABLE 5. Representative composition of garnet of the peridotite xenoliths enclosed in the Cosmos-1 (VV-02, VV-03, VV-3, VV-4, VV-5b) Carolina-1 (VV-36) and Canastra-1 (VV-31, VV-32, VV-33, VV-34) kimberlites. Structural formulas are calculated on the basis of 12 oxygens.

Sample	VV-02	VV-03	VV-03	VV-04	VV-05b	VV-36	VV-31	VV-32	VV-32	VV-33	VV-34
Location	core	rim	core	core		core	core	core	rim	core	core
Lithotype	alt	alt	alt	alt	xen	dun	lherz	harz	harz	lherz	lherz
SiO_2	41.37	41.54	42.65	41.16	41.91	42.44	42.19	42.34	42.46	42.11	41.98
TiO_2	0.09	0.77	0.79	0.84	0.58	0.39	0.00	0.00	0.00	0.01	0.03
Al_2O_3	20.23	22.51	21.40	20.07	20.93	21.44	21.29	20.79	20.87	22.63	19.95
Cr_2O_3	3.68	1.42	1.53	2.74	1.92	3.58	4.46	4.29	4.35	2.16	5.43
FeO	8.21	7.32	7.47	8.32	8.31	6.87	6.44	6.06	6.13	8.39	6.18
MgO	19.47	21.86	21.73	20.27	21.12	20.57	21.08	22.38	22.36	19.98	20.46
MnO	0.35	0.11	0.13	0.26	0.18	0.33	0.35	0.31	0.30	0.41	0.35
CaO	6.12	4.94	4.86	5.51	4.65	4.49	5.07	3.35	3.04	4.61	5.35
Na_2O	0.03	0.05	0.06	0.07	0.07	0.08	0.04	0.02	0.03	0.00	0.03
Total	99.54	100.52	100.63	99.23	99.66	100.19	100.92	99.54	99.54	100.31	99.75
Si	2.982	2.916	2.999	2.966	2.987	3.010	2.976	3.009	3.015	2.992	3.009
Ti	0.005	0.041	0.042	0.045	0.031	0.021	0.000	0.000	0.000	0.001	0.002
Al	1.718	1.862	1.774	1.704	1.758	1.792	1.770	1.741	1.747	1.895	1.685
Cr	0.210	0.079	0.085	0.156	0.108	0.201	0.249	0.241	0.244	0.121	0.308
Fe^{3+}	0.102	0.151	0.067	0.128	0.107	0.000	0.035	0.002	0.000	0.000	0.000
Fe^{2+}	0.393	0.279	0.373	0.373	0.388	0.408	0.345	0.358	0.364	0.499	0.371
Mg	2.092	2.288	2.278	2.177	2.244	2.175	2.216	2.371	2.367	2.116	2.186
Mn	0.022	0.006	0.008	0.016	0.011	0.020	0.021	0.019	0.018	0.025	0.021
Ca	0.472	0.371	0.367	0.425	0.355	0.341	0.383	0.255	0.231	0.351	0.410
Na	0.004	0.006	0.008	0.010	0.010	0.011	0.005	0.003	0.005	0.000	0.004
Total (apfu)	8.000	8.000	8.000	8.000	8.000	7.978	8.000	8.000	7.991	7.999	7.995
Hutcheonite	0.3%	2.0%	0.0%	1.7%	0.7%					0.0%	
Morimotoite			3.3%	0.1%	0.8%						
NaTi garnet			0.4%	0.5%	0.5%	0.6%					0.1%
Majorite								0.6%			
Uvarovite	10.5%	3.9%	4.3%	7.8%	5.4%	10.1%	12.4%	8.5%	7.7%	6.1%	13.7%
Knorringite								3.6%	4.5%		1.7%
Spessartine	0.7%	0.2%	0.3%	0.5%	0.4%	0.7%	0.7%	0.6%	0.6%	0.8%	0.7%
Pyrope	69.7%	76.3%	75.9%	72.6%	74.8%	72.7%	73.9%	74.7%	74.5%	70.5%	71.2%
Almandine	13.1%	9.3%	11.3%	10.4%	12.1%	13.6%	11.5%	11.8%	12.1%	16.6%	12.4%
Grossular	1.5%	3.2%	1.1%			1.2%	0.3%			5.6%	
Andradite	3.5%	3.3%	3.3%	4.4%	4.8%						
Skiagite				2.0%	0.6%			0.1%			
Khoharite											
Remainder	0.7%	1.9%	0.0%	0.0%	0.0%	1.2%	1.2%	0.2%	0.6%	0.3%	0.3%
Total	100.0%	100.0%	100.0%	100.0%	100.0%	100.0%	100.0%	100.0%	100.0%	100.0%	100.0%

int – between core and rim; dun – dunite; alt – partially altered peridotite; harz – harzburgite; lherz – lherzolite; xen - xenocryst.

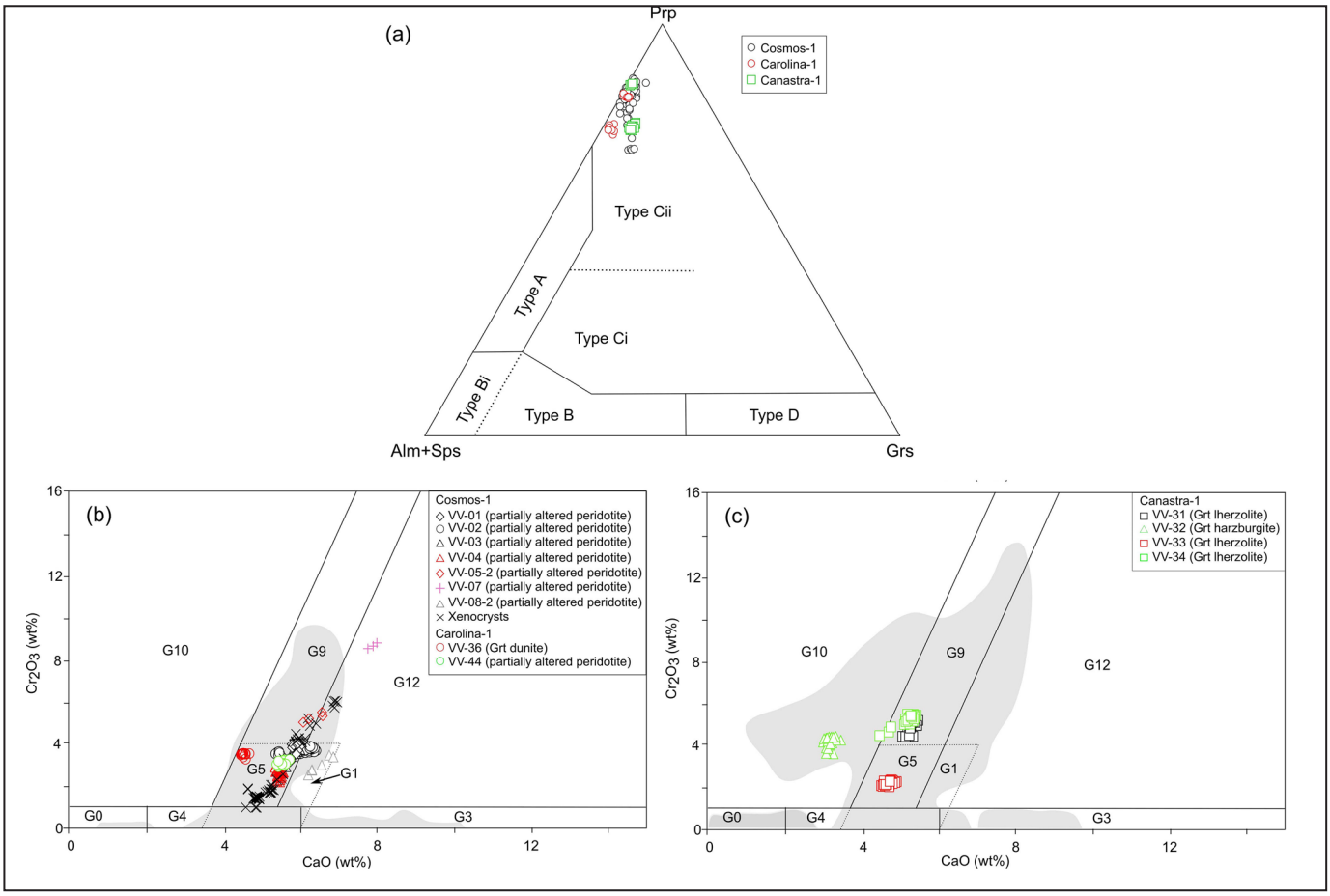

FIGURE 10 – (a) Ternary diagram showing the garnet composition with Prp (pyrope), Alm+Sps (almandine plus spessartine) and Grs (grossular) end-members; (b) CaO vs Cr_2O_3 diagram with the classification scheme of Grütter et al. (2004) showing the composition of garnet of the investigated samples from Rondônia; (c) CaO vs Cr_2O_3 diagram with the classification scheme of Grütter et al. (2004) showing the composition of garnet of the investigated samples of the Canastra-1 kimberlite. The grey areas in (b) and (c) represent the composition of garnet of the mantle xenoliths and concentrates of the kimberlites from Rondônia (1037 analyses) and APIP (2967 analyses), respectively, from previous works. Data compilation from: Esperança et al. (1995), Carvalho (1997), Zolinger (2005), Tappert et al. (2006), Chaves (2008a,b), Costa (2008), Pasin (2008), Thomaz (2009), Coelho (2010), Hunt et al. (2009), Andrade and Chaves (2011), Andrade (2012), Weska et al. (2012), Fernandes et al. (2014), Hill et al. (2015), Nannini (2016), Cabral Neto et al. (2017a) and Gervasoni et al. (2022).

10a) with Mg# from 73.5 to 84.5. There is a compositional difference among the samples, as the grains are identified as G5 (pyroxenitic), G9 (lherzolitic), G1 (low-Cr megacrysts) and G12 (wehrlitic) following the classification scheme of Grütter et al. (2004). The composition is similar to the garnet analyzed in Rondônia kimberlites by other works (Figure 10b). There is no considerable variation between the core and rim observed in X-ray compositional maps and chemical profiles (Figure 11a-d, Figure 12a). However, a slight decrease in Cr_2O_3 at the rims is observed in the chemical zoning profile present in Figure 12b. A local decrease in CaO content at the rims also occurs. The reaction rim coronas surrounding garnet often present tiny spinel grains with Cr_2O_3 content ranging from 23 to 43 wt% and Al_2O_3 from 14 to 39 wt% (Table 6). Ilmenite grains, located near the contact between the xenolith and the kimberlitic matrix, present 11 wt% of MgO. Ilmenite macrocrysts present MgO from 12 to 17 wt% (Table 6).

The garnet of the peridotite samples enclosed in Canastra-1 kimberlite is dominated by pyrope (68-77 mol%), with 10-17 mol% almandine, 5-14 mol% uvarovite and Mg# from 79.8 to 87 (Figure 10a). There is also a compositional difference between the samples, as the grains are classified as G5, G9 and G10 (harzburgite) following the classification scheme of Grütter et al. (2004) (Figure 10c). The chemical profiles performed across the grains are flat, showing locally rims with a slight increase in Cr_2O_3 content, as observed in garnet harzburgite VV-32 (Figure 12c). A decrease in Cr_2O_3 content at the rims of garnet from lherzolite locally occurs. The garnet also presents thin reaction rims with small spinel grains with Cr_2O_3 ranging from 12 (harzburgite) to 51 wt% (Table 5). Isolated spinel grains in the wehrlite VV-29 present 59 wt% of Cr_2O_3 and 4 wt% of Al_2O_3 (Table 5).

5.2. P-T calculations

The *P-T* equilibrium conditions of the mineral assemblages were determined using the PTEXL spreadsheet (available at cms.eas.ualberta.ca/team-diamond/downloads/) and PTQuick software (Simakov and Dolivo-Dobrovolsky 2009). The average compositions of the grain cores were used in the calculations. Table 7 shows the results for representative samples calculated in the PTEXL, considering pressure and temperature presets of 40 kbar and 1000 ºC, respectively.

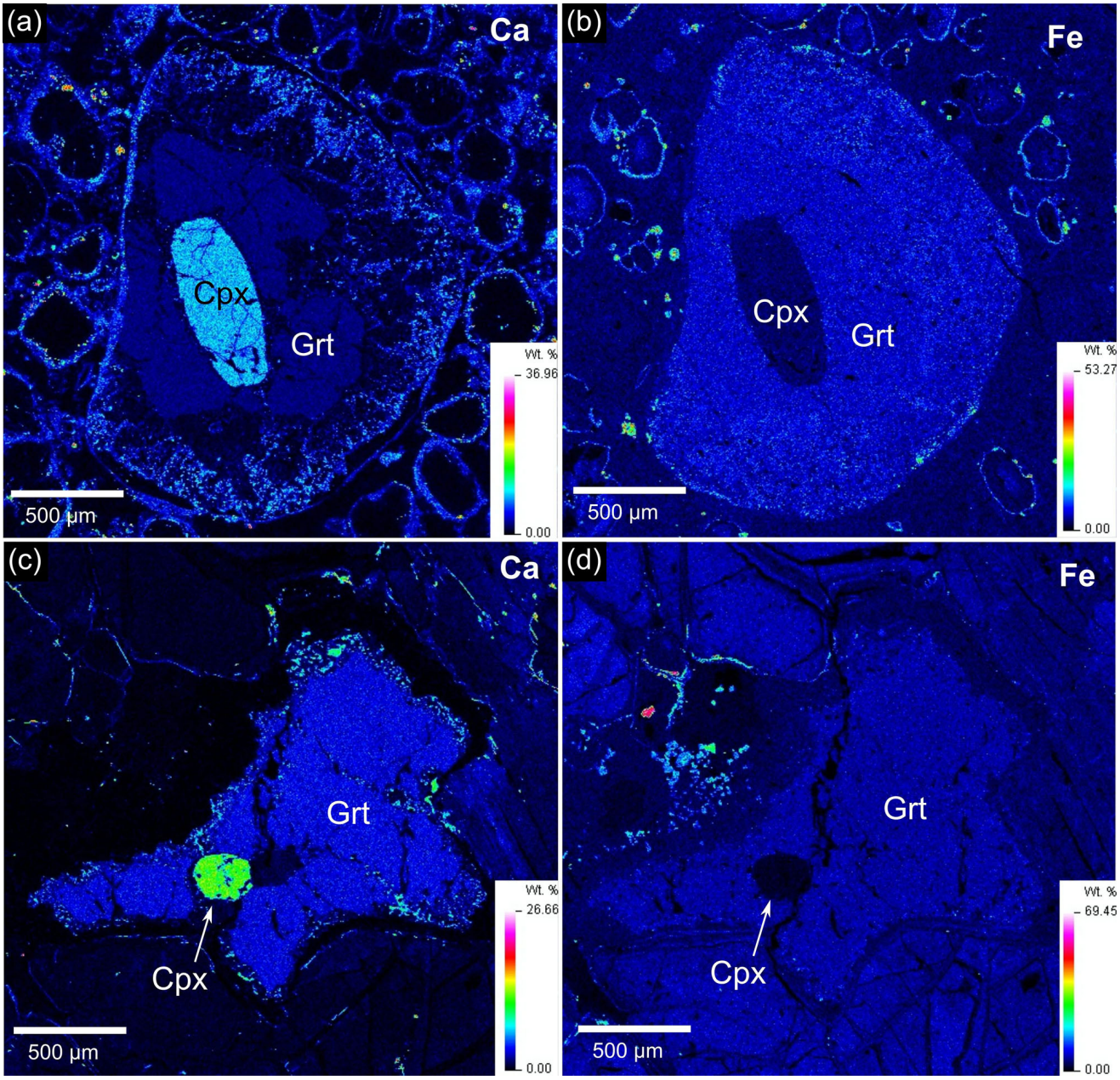

FIGURE 11 – Ca (a and c) and Fe (b and d) X-ray compositional maps of garnet (Grt) with inclusion of clinopyroxene (Cpx) enclosed in Cosmos-1 kimberlite.

The equilibrium temperatures calculated for the samples from Rondônia are higher relative to those from Minas Gerais based on the two-pyroxene thermometer of Brey and Köhler (1990) (1130 ºC vs. 879 and 1097 ºC) , the garnet-clinopyroxene thermometers of Powell (1985) (1063-1279 ºC vs 880-1160 ºC) and Ellis and Green (1979) (1063-1279 ºC vs 903-1170 ºC) and also the single clinopyroxene thermometer of Nimis and Taylor (2000) (1032-1227 ºC vs 831-989 ºC). The new calibration of Sudholz et al. (2021) for the single clinopyroxene barometer provided a higher pressure to the garnet dunite VV-36 (50 kbar) enclosed in the Carolina-1 kimberlite. However, the pressure calculated for this sample using the garnet-orthopyroxene barometers of Brey and Köhler (1990) and Nickel and Green (1985) is otherwise in the same interval calculated for the peridotites enclosed in the Canastra-1 kimberlite (38-44 kbar).

Figures 13 and 14 show the *P-T* stability fields of the peridotite samples from Rondônia and Minas Gerais, respectively, as the areas formed by the intersections of the thermometers and barometers calculated using the PTQuick software. The stability fields of the garnet dunite and the partially altered peridotite samples from Rondônia present higher pressures (40-60 kbar) and temperatures (1030-1380 ºC) relative to the those of the peridotite samples enclosed in the Canastra-1 kimberlite (25-40 kbar and 730-1000 ºC; Figure 14).

6. Discussion

6.1. Composition of the SCLM beneath the Azimuth 125º Lineament

The alkaline provinces in the Azimuth 125º Lineament represent key areas to the better understanding of the structural and compositional diversity of the SCLM beneath

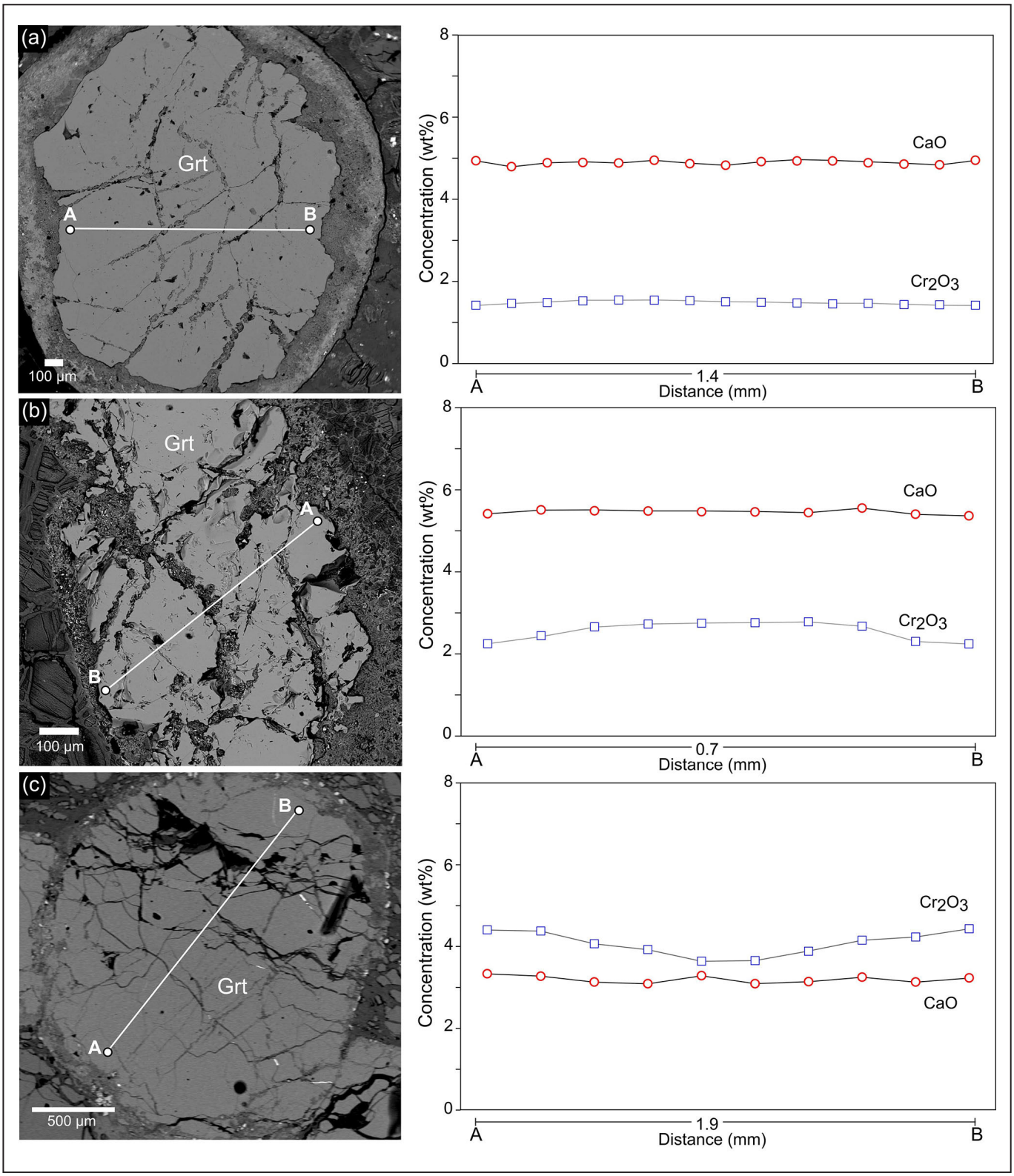

FIGURE 12 – Backscattered electron images and chemical zoning profiles of garnet (Grt) grains. (a) Garnet xenocryst in Cosmos-1 kimberlite; (b) Garnet in partially altered peridotite enclosed in Cosmos-1 kimberlite; (c) Garnet in harzburgite enclosed in the Canastra-1 kimberlite.

the Brazilian Platform. However, the amount of the data available is heterogeneous throughout the area, as the amount and distribution of major and trace element data in mantle minerals are distinct for each alkaline province. Most of the published chemical data are from the APIP (e.g., Carvalho 1997; Costa 2008; Nannini 2016) and form the compositional fields in figures 9 and 10 (2967 analyses of garnet and 1322 of clinopyroxene). Data from the Paranatinga, Juína and Rondônia kimberlite fields are less abundant (e.g., Zolinger 2005; Hunt et al. 2009; Weska et al. 2012; 1836 analyses of garnet and 815 of clinopyroxene for the three locations). Figure 15 indicates

TABLE 6. Representative composition of spinel (Sp) and ilmenite (Ilm). Spinel is located in xenoliths enclosed in the Cosmos-1 (VV-02 and VV-08) and Canastra-1 (VV-29, VV-31 and VV-32) kimberlites. Ilmenite is in the partially altered peridotite xenolith and as macrocrysts in Cosmos-1 kimberlite (VV-2, VV-07 and VV-08). Structural formulas are calculated on the basis of 4 and 3 oxygens for spinel and ilmenite, respectively.

Sample	VV-02	VV-08	VV-31	VV-31	VV-29	VV-32	VV-02	VV-07	VV-08
Mineral	Sp	Sp	Sp	Sp	Sp	Sp	Ilm	Ilm	Ilm
Lithotype	alt	alt	lherz	lherz	wehr	harz	alt	macro	macro
SiO_2	0.02	0.02	0.05	0.13	0.08	0.21		0.84	0.00
TiO_2	1.95	5.00	3.90	2.27	2.56	0.20	52.58	48.93	55.18
Al_2O_3	39.08	13.77	8.12	15.27	4.05	56.04	0.27	0.50	0.66
Cr_2O_3	22.96	42.79	51.03	48.03	59.46	12.30	4.54	8.21	1.08
Fe_2O_3*	4.93	5.40	5.91	4.64	4.14	0.60	2.40	6.89	4.28
FeO	13.37	19.20	18.42	15.97	16.78	7.34	26.94	17.55	22.26
MnO	0.37	0.39	0.34	0.28	0.33	0.15	0.64	0.55	0.36
MgO	17.02	12.14	11.58	13.18	11.37	21.78	11.04	15.10	15.15
ZnO	0.00	0.08	0.08	0.07	0.11	0.04	0.05	0.00	
NiO	0.08	0.10	0.16	0.14	0.15	0.08	0.11	0.21	0.15
Total	99.78	98.88	99.59	99.97	99.03	98.74	98.57	98.77	99.12
Si	0.001	0.001	0.002	0.004	0.003	0.005	0.000	0.019	0.000
Ti	0.041	0.122	0.097	0.054	0.065	0.004	0.932	0.840	0.944
Al	1.299	0.526	0.317	0.570	0.162	1.717	0.008	0.013	0.018
Cr	0.512	1.097	1.338	1.203	1.596	0.253	0.085	0.148	0.019
Fe^3	0.105	0.132	0.147	0.111	0.106	0.012	0.043	0.118	0.073
Fe^2	0.315	0.521	0.511	0.423	0.476	0.160	0.531	0.335	0.423
Mn	0.009	0.011	0.010	0.008	0.009	0.003	0.013	0.011	0.007
Mg	0.716	0.587	0.572	0.622	0.575	0.844	0.388	0.513	0.514
Zn	0.000	0.002	0.002	0.002	0.003	0.001	0.001	0.000	0.000
Ni	0.002	0.003	0.004	0.004	0.004	0.002	0.002	0.004	0.003
Total	3.000	3.002	3.000	3.001	2.999	3.001	2.001	2.001	2.001

alt – partially altered peridotite; wehr – wehrlite; harz – harzburgite; lherz – lherzolite; macro – macrocryst.
*calculated according to Droop (1987)

TABLE 7. *P-T* calculations of the PTEXCL spreadsheet of peridotite samples enclosed in Cosmos-1 (VV-01, VV-02, VV-03, VV-04, VV-5b), Carolina-1 (VV-36) and Canastra-1 (VV-29, VV-31, VV-32, VV-33, VV-34) kimberlites. Temperatures are in ºC, and pressures in kbar.

Sample	VV-01	VV-02	VV-03	VV-04	VV-05b	VV-36	VV-29	VV-31	VV-32	VV-33	VV-34
Lithotype	alt	alt	alt	alt	xen	dun	wehr	lherz	harz	lherz	lherz
T_{BK90}						1130.9				879.4	1097.4
T_{NG10}						997.9		939.8	923.6	852.5	977.6
T_{EG79}	1233.9	1062.6	1225.6	1238.6	1279.2	1139.5				903.2	1170.2
T_{P85}	1227.5	1046.8	1218.7	1232.3	1275.3	1126.8				879.9	1159.8
$T_{NT-00-T}$	1226.9		1137.9	1117.7	1214.1	1032.5				831.1	989.2
P_{BK90}						41.3		41.0	37.8	43.3	38.7
P_{NG85}						43.0		42.9	41.2	43.6	41.3
$P_{NT100-P}$	31.4	40.4	40.8	40.2	37.7	45.2				40.7	42.6
P_{S21}	33.1	43.4	45.6	46.4	43.5	50.0				43.4	45.5

alt – partially altered peridotite; wehr – wehrlite; harz – harzburgite; lherz – lherzolite; dun – dunite; xen – garnet xenocryst with inclusion of clinopyroxene.
T_{BK90}: Two pyroxene Brey and Koehler (1990); T_{NG10}: Nimis and Grütter (2010); T_{EG79}: Ellis and Green (1979); T_{P85}: Powell (1985); $T_{NT-00-T}$: Nimis and Taylor (2000); P_{BK90}: Garnet-orthopyroxene Brey and Koehler (1990); P_{NG85}: Nickel and Green (1985); $P_{NT100-P}$: Nimis and Taylor (2000); P_{S21}: Sudholz et al. (2021).

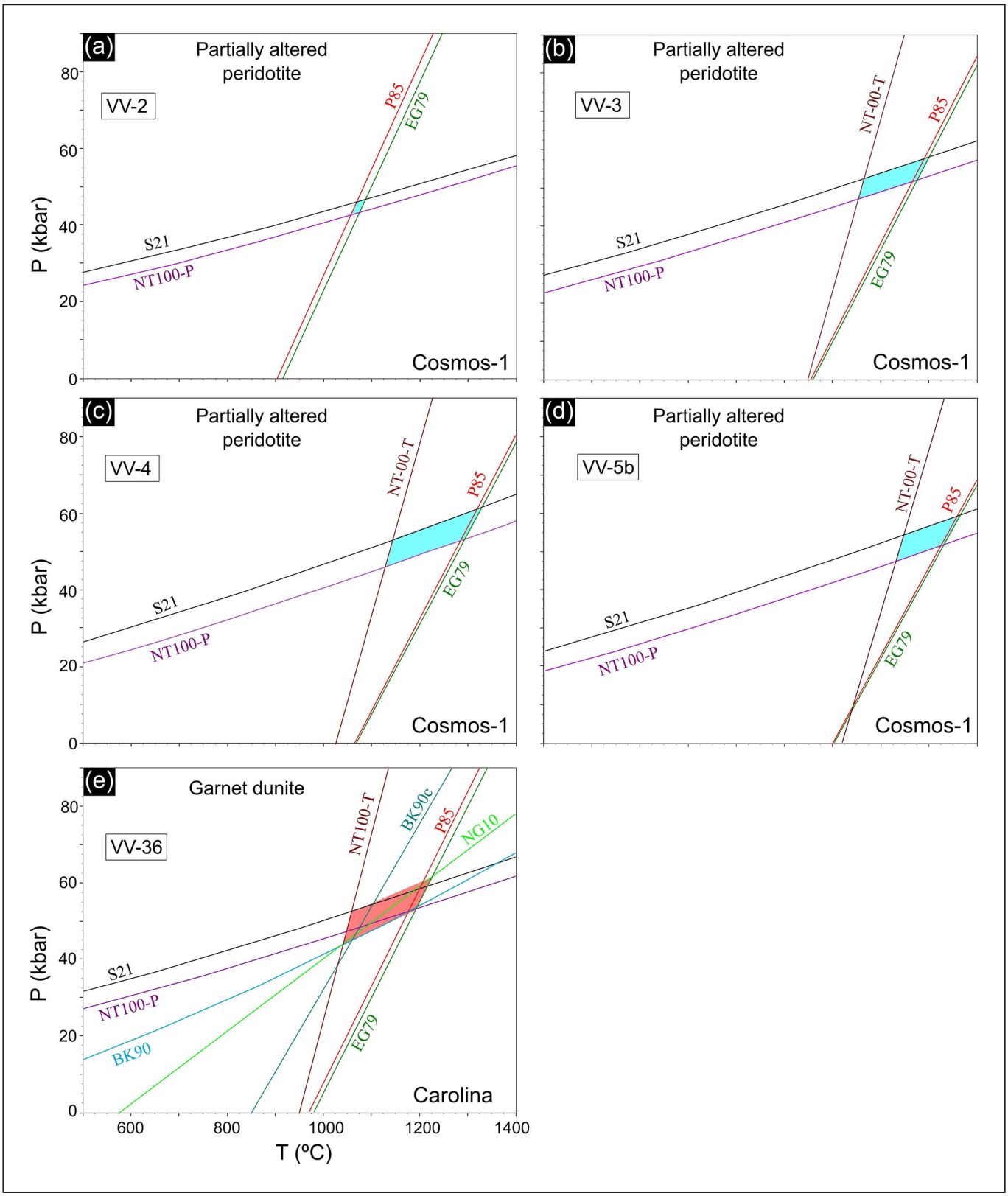

FIGURE 13 – P-T diagrams showing the stability fields (blue and red) generated by the intersections of the thermometers and barometers used in PTQuick software (Simakov and Dolivo-Dobrovolsky 2009) for the peridotite samples from Rondônia. T_{BK90c}: Two pyroxene Brey and Köhler (1990); T_{NG10}: Nimis and Grütter (2010); T_{EG79}: Ellis and Green (1979); T_{P85}: Powell (1985); $T_{NT-00-T}$: Nimis and Taylor (2000); P_{BK90}: Garnet-orthopyroxene Brey and Köhler (1990); $P_{NT100-P}$: Nimis and Taylor (2000); P_{S21}: Sudholz et al. (2021).

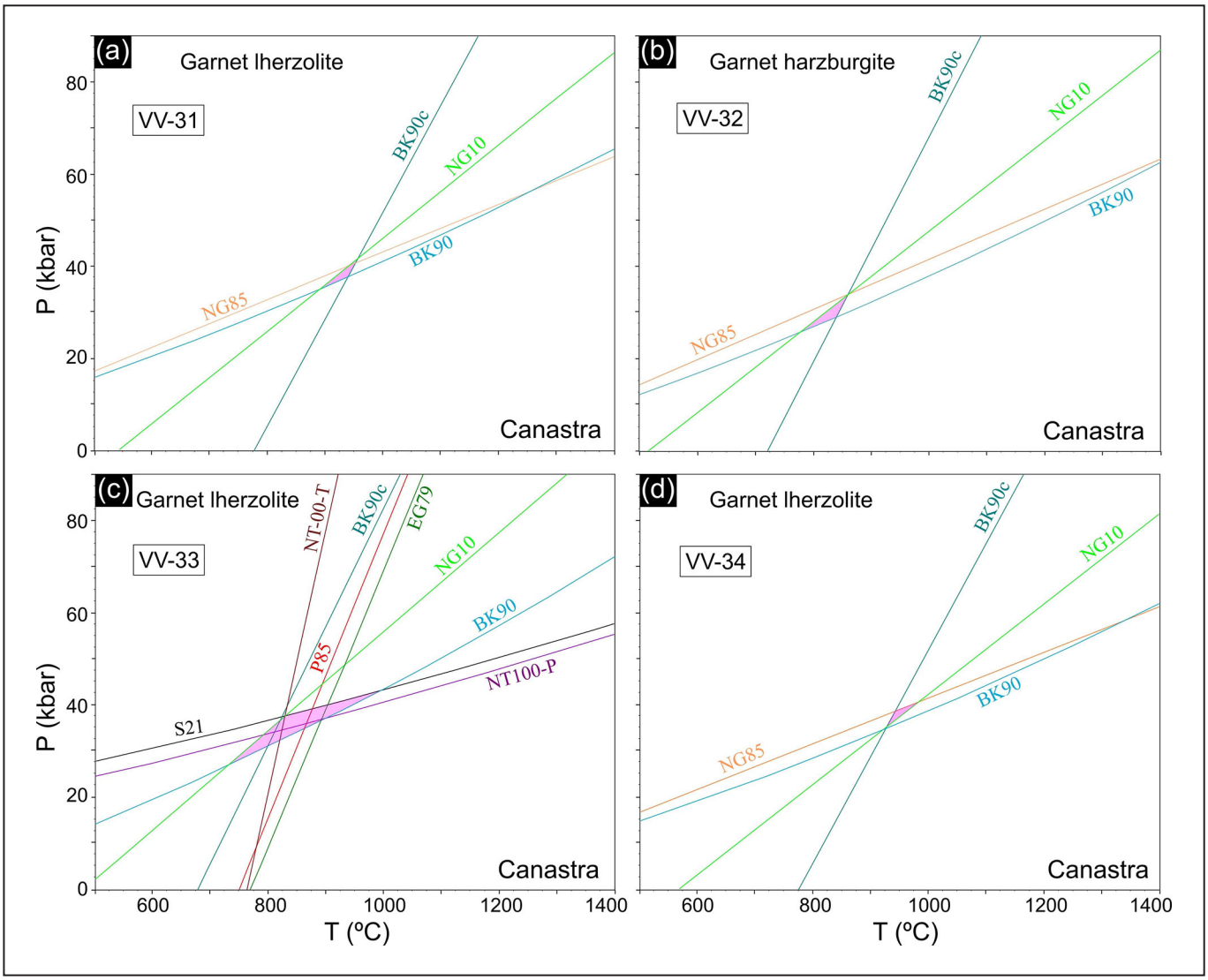

FIGURE 14 – P-T diagrams showing the stability fields (pink) generated by the intersections of the geothermometers and geobarometers used in PTQuick software (Simakov and Dolivo-Dobrovolsky 2009) for the peridotite samples enclosed in Canastra-1 kimberlite. T_{BK90c}: Two pyroxene Brey and Köhler (1990); T_{NG10}: Nimis and Grütter (2010); T_{EG79}: Ellis and Green (1979); T_{P85}: Powell (1985); $T_{NT-00-T}$: Nimis and Taylor (2000); P_{BK90}: Garnet-orthopyroxene Brey and Köhler (1990); $P_{NT100-P}$: Nimis and Taylor (2000); P_{S21}: Sudholz et al. (2021).

the higher abundance of harzburgite G10 garnet in the area of the APIP relative to the other provinces located in the Amazonian Craton (Figure 15b-c). The subcalcic G10 garnet is typical of SCLM beneath areas older than 2.5 Ga and is traditionally linked with diamond deposits (Sobolev et al. 1973; Pearson et al. 2014a). Its presence in the APIP can be related to the remnants of the Archean lithospheric mantle in the area, as highlighted by previous works through Os isotopes, geophysics and microstructural data on mantle xenoliths (e.g., Carlson et al. 2007; Fernandes et al. 2021). The occurrence of G10 garnet in the Amazonian Craton is rare and only described in few works (Maunula 2006; Bulanova et al. 2008; Oliveira et al. 2019). The G10 garnet was only found in a harzburgite xenolith (VV-32) studied in the present work from the diamond-bearing Canastra-1 kimberlite (Figure 10c). The garnets from Rondônia are mostly G5 (pyroxenitic) and G9 (lherzolitic) (figure 10b). In this case, the terranes of the Amazonian Craton, in which the kimberlite pipes are emplaced, are part of the Paleo to Mesoproterozoic southwestern geochronological provinces with no involvement of an Archean crust (1.8-1.0 Ga; Rio Negro-Juruena, Rondoniano-San Ignácio and Sunsás; Tassinari and Macambira 1999). In fact, the G10 garnet is considered less common in terranes with ages from 2.5 to 1 Ga worldwide (Griffin et al. 1999; Pearson et al. 2014a). Figures 15 and 16 indicate the higher abundance of G3 and G4 garnet and lower-Cr_2O_3 clinopyroxene with eclogitic composition in the Amazonian Craton relative to the APIP, which can be related to a distinct tectonothermal evolution of each area. Although the southwestern portion of the Amazonian Craton presents an extensively tectonic evolution in the Precambrian, the eclogitic garnet of the area is considered by Gervasoni et al. (2022) as the record of a Paleozoic subduction in western South America. These tectonic processes beneath the Amazonian Craton can result in the deformation observed in some mantle xenoliths. Microstructural and chemical data indicate that the Cretaceous magmatism of the APIP is related to the development of the porphyroclastic textures of peridotites beneath the area (e.g., Fernandes et al. 2021).

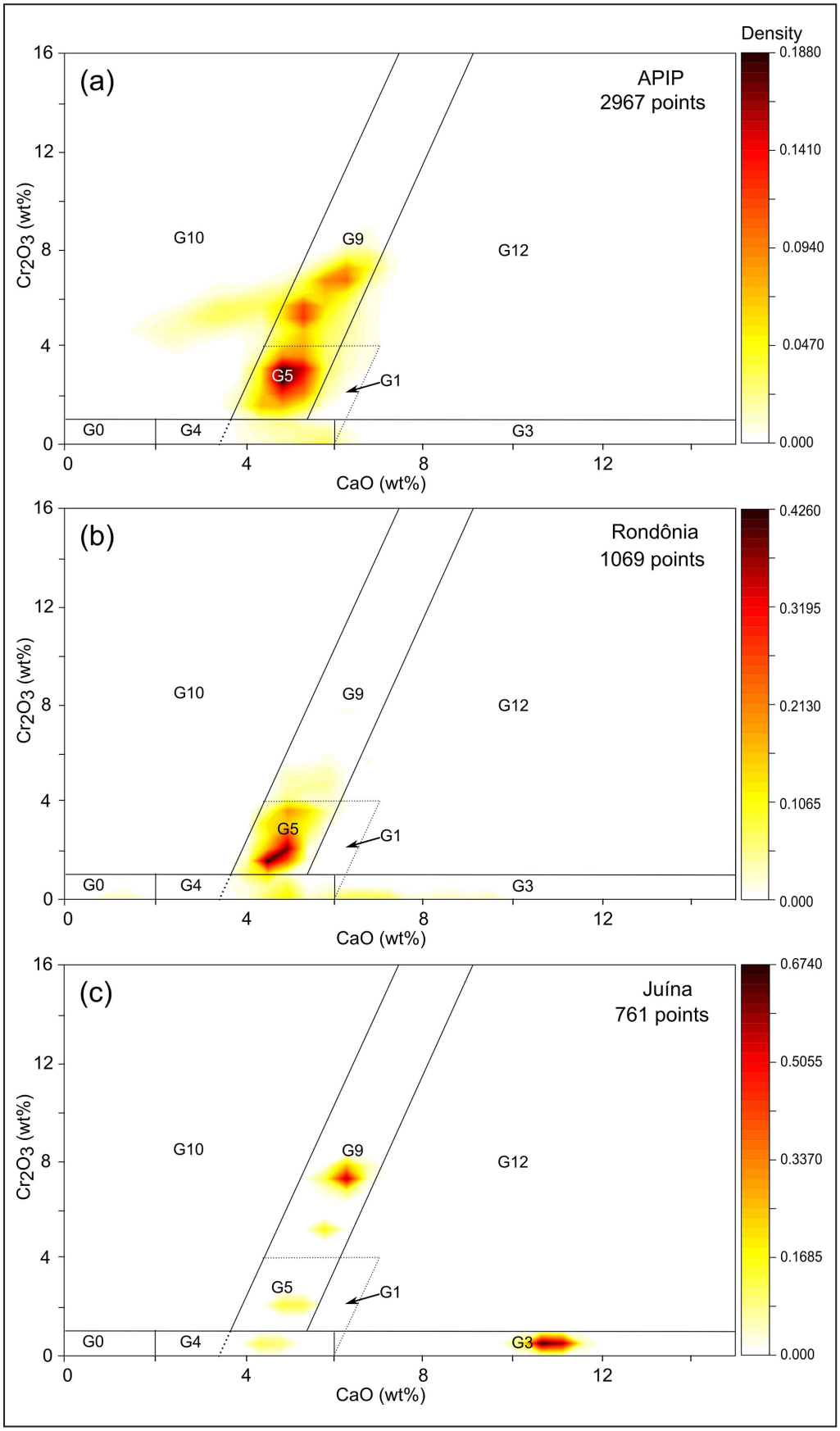

FIGURE 15 – Density diagrams using garnet compositions of the kimberlite fields along the Azimuth 125º Lineament from APIP (a), Rondônia (b) and Juína (c). Data compiled from: Esperança et al. (1995), Costa (1996), Carvalho (1997), Zolinger (2005), Tappert et al. (2006), Chaves (2008a,b), Costa (2008), Pasin (2008), Thomaz (2009), Coelho (2010), Hunt et al. (2009), Andrade and Chaves (2011), Andrade (2012), Weska et al. (2012), Costa (2013), Fernandes et al. (2014), Hill et al. (2015), Nannini (2016), Cabral Neto et al. (2017b), Gervasoni et al. (2022).

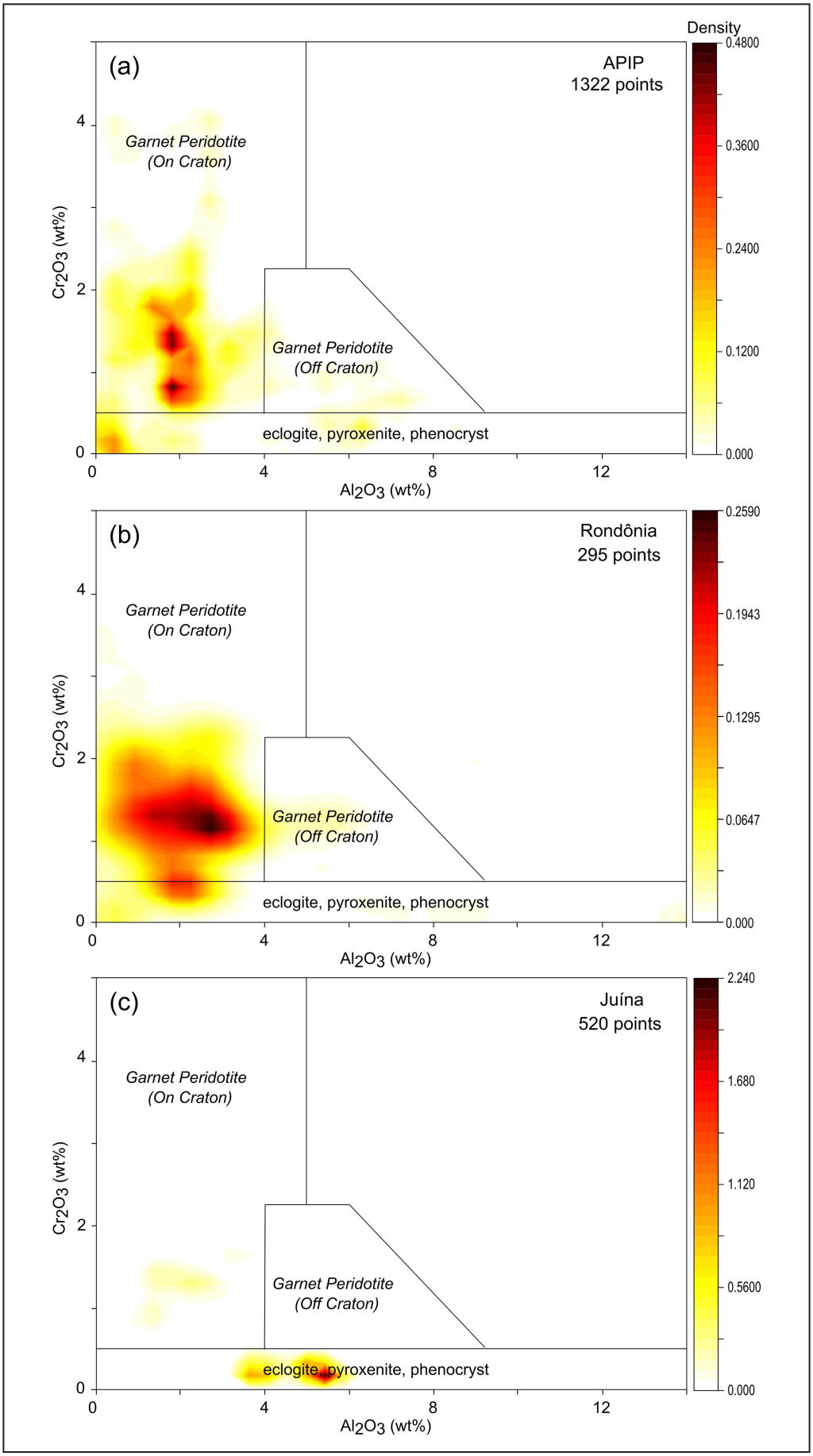

FIGURE 16 – Density diagrams using clinopyroxene compositions of the kimberlite fields along the Azimuth 125º Lineament. APIP (a), Rondônia (b) and Juína (c). Data compiled from the same references present in Figure 15.

6.2. Geothermal gradients

Figure 17 shows that the *P-T* stability fields of the peridotite xenoliths enclosed in the Canastra-1 kimberlite are close to the 40 mW/m^2 geotherm, considering the geothermal gradients after Hasterok and Chapman (2011). The *P-T* calculations obtained by Costa (2008) in the peridotite xenoliths enclosed in the same kimberlite also plot near the 40 mW/m^2 geotherm, but in higher pressure and temperature conditions in the diamond stability field (Figure 17). These data are, for the most part, included in the field formed by the *P-T* calculations of Read et al. (2004) based on the composition of clinopyroxene of the APIP. Spinel peridotites of the APIP are equilibrated along a warmer geotherm (40-50 mW/m2), according to Cabral Neto et al. (2017b) and Fernandes et al. (2021).

The *P-T* stability fields of the peridotite samples from Rondônia are aligned near the cratonic 40 mW/m^2 geotherm in the diamond stability field, except for the partially altered peridotite xenolith VV-02. The data is distinct from those obtained by Costa (2013) in peridotite xenoliths enclosed in Juína kimberlites, as the *P-T* estimates are located closer to the 50 mW/m^2 geotherm (Figure 17). Considering that the Juína kimberlites are younger than the occurrences from Rondônia (80-90 Ma *vs.* ca. 260-240 Ma; Heaman et al. 1998; Kaminski et al. 2010; Felgate 2014), a change of the geothermal gradient may have occurred in the southwestern portion of the Amazonian Craton after the Permian-Triassic. This modification in the geothermal gradient from a 38 mW/m^2 to a 44 mW/m^2 geotherm is also constrained by Hunt et al. (2009) based on the *P-T* conditions of clinopyroxene xenocrysts of the Carolina kimberlite and from possibly younger Cretaceous-Tertiary kimberlites located at the Pimenta Bueno kimberlite field. The data obtained in this work reinforces the occurrence of the cratonic 40 mW/m^2 geothermal gradient in the region that may be related to a process by thermal relaxation of the lithospheric mantle after the Paleo to Mesoproterozoic tectonothermal events of the southwestern Amazonian Craton until the sampling of the xenoliths by the magma in the Permian-Triassic. This process is reported worldwide through the study of mantle xenoliths (e.g., Pintér et al. 2015; Guo et al. 2019; Afonso et al. 2022).

6.3. Implications to diamond occurrences

Diamond placer deposits have been mined in Minas Gerais state since the 18th century, when Brazil was the main diamond producer in the world, while the first record of detrital diamond in Rondônia state is dated from the beginning of the 20th century (e.g., Svisero 1995, Tappert et al. 2006, Karfunkel et al. 2014, Cabral Neto et al. 2017b, Giuliani and Pearson 2019). The discovery of mineralized kimberlite pipes is more recent and Canastra-1 is the first with recognizable economic interest (e.g., Chaves et al. 2008 a,b). The knowledge is limited on the kimberlitic sources of the placer deposits and the theme is still under discussion (e.g., Tappert et al. 2006; Karfunkel et al. 2014, Pereira et al. 2017). The distinct composition of the SCLM along the Azimuth 125º Lineament indicates that different mantle sources can be related to the origin of the diamond that occur in the studied area. The higher abundance of G10 garnet in the APIP and the presence of remnants of an Archean cratonic lithospheric mantle indicate a potential for the occurrence of diamond from a harzburgitic source, as

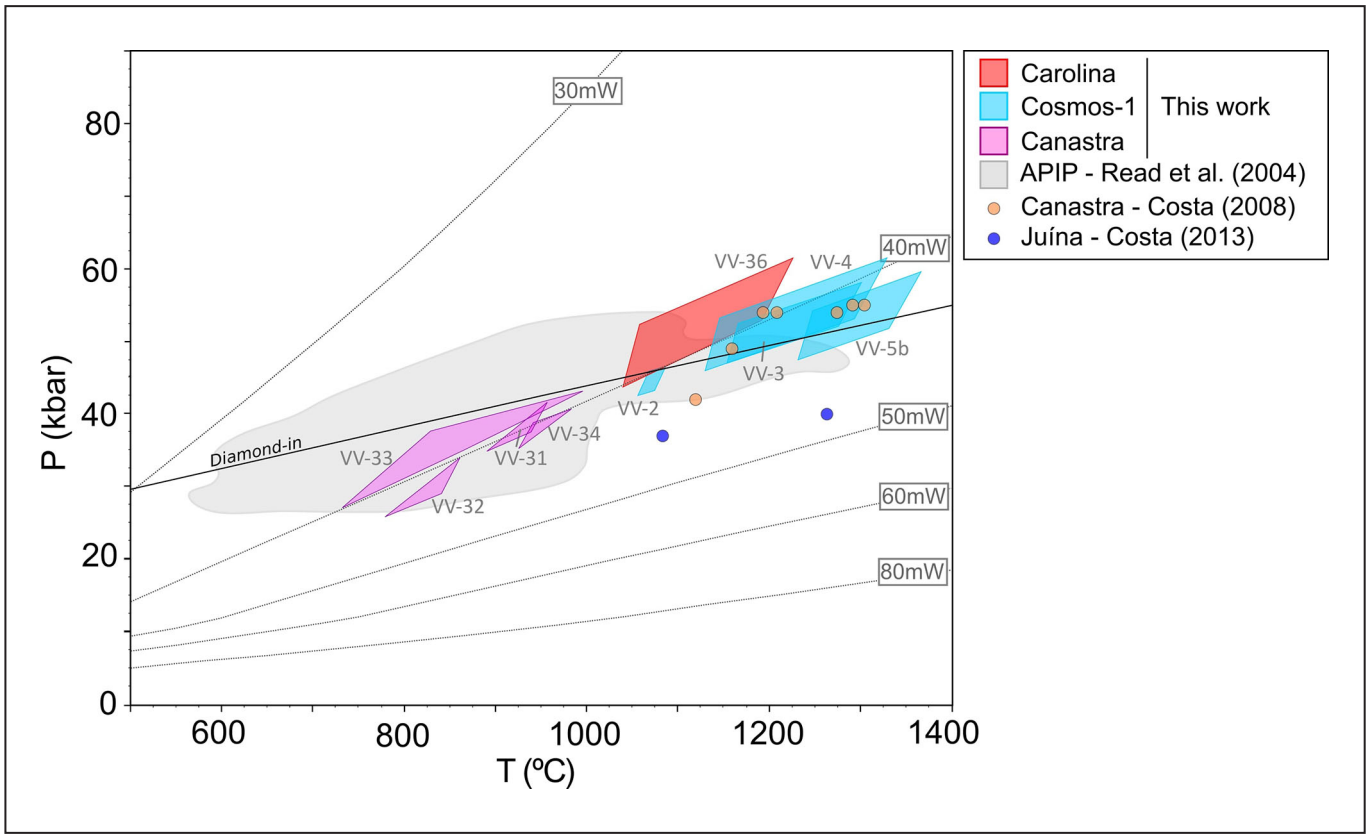

FIGURE 17 – Geothermal gradients after Hasterok and Chapman (2011) and P-T stability fields calculated from the investigated mantle xenoliths of the present work in comparison with the data obtained from previous works on the Azimuth 125º Lineament.

seen in other provinces worldwide (e.g., Klein-BenDavid and Pearson 2009). In fact, the diamond from alluvial deposits of the Serra da Canastra present inclusions with depleted composition (Tappert et al. 2006). However, recent studies have demonstrated that a high proportion of lherzolitic and eclogitic diamonds occur in the alluvial deposits of Verde River, Abaeté and Douradinho River also in the APIP area, with evidence for the presence of subduction zones and recycled crustal material in the mantle during the Paleoproterozoic (Carvalho et al. 2022). Deposits with the predominance of eclogitic diamonds occur in the southwestern Amazonian Craton, like the one located in the Carolina-1 kimberlite (Hunt et al. 2009). The same is constrained in Juína, with evidence for the contribution of slab melts in the origin of the sublithospheric diamonds (Kaminski et al. 2008, Thomsom et al. 2016). Indeed, deposits with the predominance of eclogitic diamonds are generally located at the margin of cratons or in areas with tectonothermal history younger than Archean (Stachel and Harris 2008), like the southwestern Amazonian Craton. However, the peridotite xenoliths from Rondônia investigated in this work show *P-T* equilibrium conditions in the diamond stability field and may also be the source of at least part of the diamond from the area. This possibility can be further investigated with more data on the diamond and mantle xenoliths from the Amazonian Craton.

7. Conclusions

The peridotite xenoliths enclosed in kimberlites from Rondônia and Minas Gerais (APIP) present distinct mineral compositions related to the diversity of the SCLM along the Azimuth 125º Lineament, with areas located in the southwestern portion of the Amazonian Craton and the Brasília Belt, respectively. The new chemical data together with a comprehensive compilation of the previous works indicate that the harzburgite G10 garnet occurs in the area of the APIP in higher abundance relative to the other provinces located in the Amazonian Craton. Its presence in the APIP can be considered as evidence for the presence of remnants of the Archean root of the São Francisco Craton beneath the area. The *P-T* conditions calculated for the samples from Rondônia present higher pressures (40-60 kbar) and temperatures (1030-1380 ºC) relative to the samples enclosed in the Canastra-1 kimberlite (25-40 kbar and 730-1000 ºC, respectively). However, the calculated *P-T* stability fields of the xenoliths from both locations are aligned close to the 40 mW/m^2 geotherm. The cratonic 40 mW/m^2 geothermal gradient in Rondônia may be related to the thermal relaxation of the lithospheric mantle after the Paleo to Mesoproterozoic tectonothermal events of the southwestern Amazonian Craton until the sampling of the xenoliths by the kimberlite in the Permian-Triassic.

Acknowledgements

The authors thank to Dr. Frederico Meira Faleiros for the help with the calculations of the thermobarometric data and for commentary and suggestions in a previous version of the manuscript. The identification and sampling of mantle xenoliths from drill cores, thin section preparation and electron microprobe analyses of the mineral phases were performed with the financial support of the Geological Survey of Brazil as part of the project 4432.084 “Study of the subcontinental lithospheric mantle (SCLM) beneath the Azimuth 125º Lineament through deep geophysics and mineralogical and petrographical characterization of mantle xenoliths” that has been developed by the Division of Geodynamics since 2019. The paper was substantially improved following comments and suggestions by Felix Kaminsky and an anonymous reviewer. We thank Chris Harris for the editorial handling.

Authorship credits

Author	A	B	C	D	E	F
VVA						
JBR						
ICN						
FVS						
HBS						

A - Study design/Conceptualization **B** - Investigation/Data acquisition
C - Data Interpretation/ Validation **D** - Writing
E - Review/Editing **F** - Supervision/Project administration

References

Afonso J.C., Ben-Mansour W., O´Reilly S.Y., Griffin W.L., Salajeghegh F., Foley S., Begg G., Selway K., Macdonald A., Januszczak N., Fomin I., Nyblade A.A., Yang Y. 2022. Thermochemical structure and evolution of cratonic lithosphere in central and southern Africa. Nature Geoscience, 15(5), 405-410. https://doi.org/10.1038/s41561-022-00929-y

Almeida V.V. 2009. Mineralogia e petrologia de xenólitos mantélicos das regiões de Ubatuba (SP) e Monte Carmelo (MG): evidências de fusão parcial e metassomatismo no manto superior do sudeste do Brasil. MSc Dissertation, Instituto de Geociências, Universidade de São Paulo, São Paulo, 112 p. Available online at: https://www.teses.usp.br/teses/disponiveis/44/44143/tde-14102009-082110/pt-br.php / (accessed on 24 October 2022).

Almeida V.V., Janasi V.A., Svisero D.P., Nannini F. 2014. Mathiasite-loveringite and priderite in mantle xenoliths from the Alto Paranaíba Igneous Province, Brazil: genesis and constraints on mantle metasomatism. Central European Journal of Geosciences, 6(4), 614-632. https://doi.org/10.2478/s13533-012-0197-5

Andrade K.W., Chaves M.L.S.C. 2011. Geologia e mineralogia do Kimberlito Grota do Cedro (Coromandel, MG). Geonomos, 19(1), 39-45. https://doi.org/10.18285/geonomos.v19i1.61 .

Andrade K.W. 2012. Química de Minerais indicadores de intrusões kimberlíticas com ênfase na Província Diamantífera Serra da Canastra (MG): importância na prospecção de intrusões férteis. MSc Dissertation, Instituto de Geociências, Universidade Federal de Minas Gerais, Belo Horizonte, 145 p. Available online at: http://hdl.handle.net/1843/MPBB-8YYFRZ / (accessed on 24 October 2022).

Bardet M.G. 1977. Géologie du Diamant. Troisime partie: Gisements de diamants d’Asie, d’Amérique, d’Europe et d’Australasie. Memoires du BRGM, 83, Paris, Éditions B.R.G.M., 169 p.

Borges M.P.A.C., Moura M.A., Lenharo S.L.R., Smith C.B., Araujo D.P. 2016. Mineralogical characterization of diamonds from Roosevelt Indigenous Reserve, Brazil, using non-destructive methods. Lithos, 265, 182-198. https://doi.org/10.1016/j.lithos.2016.08.003 .

Brey G.P., Köhler T. 1990. Geothermobarometry in four-phase lherzolites II: New thermobarometers and practical assessment of existing thermobarometers. Journal of Petrology, 31(6), 1353-1378. https://doi.org/10.1093/petrology/31.6.1353 .

Bulanova G.P., Smith C.B., Kohn S.C., Walter M.J., Gobbo L., Kearns S. 2008. Machado River, Brazil – a newly recognised ultradeep diamond occurrence. In: International Kimberlite Conference, 9, 9IKC-A-00233. https://doi.org/10.29173/ikc3471 .

Cabral Neto I., Nannini F., Silveira F.V., Cunha L.M., Castro C.C. 2017a. Áreas kimberlíticas e diamantíferas do estado de Rondônia. Informe de Recursos Minerais, Série Pedras Preciosas, 11, Brasília, CPRM,

85 p. Available online at: https://rigeo.cprm.gov.br/handle/doc/17617 / (accessed on 24 October 2022).

Cabral Neto I., Nannini F., Silveira F.V., Cunha L.M. 2017b. Áreas kimberlíticas e diamantíferas do estado de Minas Gerais e regiões adjacentes. Informe de Recursos Minerais, Série Pedras Preciosas, 10, Brasília, CPRM, 230 p. Available online at: https://rigeo.cprm.gov.br/handle/doc/17615 / (accessed on 24 October 2022).

Carlson R.W., Esperança S., Svisero D.P. 1996. Chemical and Os isotopic study of Cretaceous potassic rocks from Southern Brazil. Contributions to Mineralogy and Petrology, 125, 393-405. https://doi.org/10.1007/s004100050230 .

Carlson R.W., Araújo A.L.N., Junqueira-Brod T.C., Gaspar J.C., Brod J.A., Petrinovic I.A., Hollanda M.H.B.M., Pimentel M.M., Sichel S. 2007. Chemical and isotopic relationships between peridotites xenoliths and mafic-ultrapotassic rocks from Southern Brazil. Chemical Geology, 242(3–4), 415–434. https://doi.org/10.1016/j.chemgeo.2007.04.009 .

Carvalho W.T., Bressan S.R. 1981. Depósitos minerais associados ao Complexo ultramáficoalcalino de Catalão I - Goiás. In: Schmaltz W.H. (ed.). Os principais depósitos minerais da Região Centro Oeste. Brasília, DNPM, p. 139-183.

Carvalho J.B. 1997. Petrologia de xenólitos mantélicos da Província do Alto Paranaíba, Minas Gerais. PhD Thesis, Instituto de Geociências, Universidade de Brasília, Brasília, 395 p.

Carvalho L.D.V., Stachel T., Pearson D.G., Fuck R.A., Jalowitzki T., Timmerman S., Steele-MacInnis M., Gonçalves G.O., Pereira R.S., Scholz R. 2022. Diamond formation beneath the Coromandel area, southwestern São Francisco Craton – The role of refertilization and subduction. Lithos, 430-431, 106856. https://doi.org/10.1016/j.lithos.2022.106856 .

Chaves M.L.S.C., Benitez L., Brandão P.R.G., Girodo A.C. 2008a. Kimberlito Canastra-1 (São Roque de Minas, MG): geologia, mineralogia e reservas diamantíferas. REM-Revista da Escola de Minas, 61(3), 357-364. https://doi.org/10.1590/S0370-44672008000300014 .

Chaves M.L.S.C., Andrade K.W., Brandão P.R.G., Benitez L. 2008b. Província Diamantífera da Serra da Canastra e o kimberlito Canastra-1: primeira fonte primária de diamantes economicamente viável do país. Geociências, São Paulo, 27(3), 299-317. Available online at: https://www.ppegeo.igc.usp.br/index.php/GEOSP/article/view/7063/6508 / (accessed on 25 October 2022).

Chaves M.L.S.C., Andrade K.W., Moreira L.A. 2009. A intrusão diamantífera Abel Régis: kimberlito ou lamproíto? REM-Revista da Escola de Minas, 62(4), 431-438. https://doi.org/10.1590/S0370-44672009000400004 .

Coelho F.M. 2010. Aspectos Geológicos e Mineralógicos da mina de diamantes de Romaria, Minas Gerais. MSc Dissertation, Instituto de Geociências, Universidade de São Paulo, São Paulo, 105 p. https://doi.org/10.11606/D.44.2010.tde-24022011-113204 .

Cordani U.G., Ramos V.A., Fraga L.M., Cegarra M., Delgado I., de Souza K.G., Gomes F.E.M., Schobbenhaus C. 2016. Tectonic Map of South America. 2nd ed. Paris, CGMW, CPRM, SEGEMAR. Available online at: https://rigeo.cprm.gov.br/handle/doc/16750 / (accessed on 28 October 2022).

Cordeiro P.F.O., Brod J.A., Dantas E.L., Barbosa E.S.R. 2010. Mineral chemistry, isotope geochemistry and petrogenesis of niobium-rich rocks from the Catalão I carbonatitephoscorite complex, Central Brazil. Lithos, 118(3-4), 223-237. https://doi.org/10.1016/j.lithos.2010.04.007 .

Cordeiro P.F.O., Brod J.A., Palmieri M., Oliveira C.G., Barbosa E.S.R., Santos R.V., Gaspar J.C., Assis L.C. 2011. The Catalão I niobium deposit, central Brazil: Resources, geology and pyrochlore chemistry. Ore Geology Reviews, 41(1), 112-121. https://doi.org/10.1016/j.oregeorev.2011.06.013 .

Costa V.S. 1996. Estudos mineralógicos e químicos do kimberlito Batovi 6 (MT) em comparação com as intrusões Três Ranchos 4 (GO) e Limeira 1 (MG). MSc Dissertation, Instituto de Geociências, Universidade de Campinas, Campinas, 112 p. https://doi.org/10.47749/T/UNICAMP.1996.781829 .

Costa G.V. 2008. Química Mineral e geotermobarometria de xenólitos mantélicos do Kimberlito Canastra-01. MSc Dissertation, Instituto de Geociências, Universidade de Brasília, Brasília, 137 p. Available online at: https://repositorio.unb.br/handle/10482/4871 / (accessed on 25 October 2022).

Costa V.S. 2013. Mineralogia e petrologia de xenólitos mantélicos da província kimberlítica de Juína, MT. PhD Thesis, Instituto de Geociências, Universidade de São Paulo, São Paulo, 447 p. https://doi.org/10.11606/T.44.2013.tde-15052014-094703

Droop G.T.R. 1987. A General equation for estimating Fe3+ concentrations in ferromagnesian silicates and oxides from microprobe analyses, using stoichiometric criteria. Mineralogical Magazine, 51(361), 431–435. https://doi.org/10.1180/minmag.1987.051.361.10 .

Ellis D.J., Green D.H. 1979. An Experimental Study of the Effect of Ca Upon Garnet-Clinopyroxene Fe-Mg Exchange Equilibria. Contributions to Mineralogy and Petrology, 71, 13-22. https://doi.org/10.1007/BF00371878 .

Esperança S., Murray D.C., Lambert D.D., Svisero D.P. 1995. The major and trace element geochemistry of garnets from the Vargem 1 kimberlite pipe, Minas Gerais, Brazil. Anais da Academia Brasileira de Ciências, 67, 293-306.

Felgate M.R. 2014. Improved geochemical and geochronological constraints on magmatism in Rondonia and the Alto Paranaíba Igneous Province. PhD Thesis, School of Earth Sciences, University of Melbourne, Melbourne, 275 p.

Fernandes A.F., Karfunkel J., Hoover D.B., Sgarbi P.B.A., Sgarbi G.N.C.,Oliveira G.D., Gomes J.C.S.P., Kambrock K. 2014 O conglomerado basal da Formação Capacete (Grupo Mata da Corda) e sua relação com as distribuições de diamantes em Coromandel, Minas Gerais, Brasil. Brazilian Journal of Geology, 44(1), 91-103. http://dx.doi.org/10.5327/Z2317-4889201400010008 .

Fernandes P.R., Tommasi A., Vauchez A., Neves S.P., Nannini F. 2021. The São Francisco cratonic root beneath the Neoproterozoic Brasilia belt (Brazil): Petrophysical data from the kimberlite xenoliths. Tectonophysics, 816, 229011. https://doi.org/10.1016/j.tecto.2021.229011 .

Gervasoni F., Jalowitzki T., Rocha M.P., Weska R.K., Novais-Rodrigues E., Rodrigues R.A.F., Bussweiler Y., Barbosa E.S.R., Berndt J., Dantas E.L., Souza V.S., Klemme S. 2022. Recycling process and proto-kimberlite melt metasomatism in the lithosphere-asthenosphere boundary beneath the Amazonian Craton recorded by garnet xenocrysts and mantle xenoliths from the Carolina kimberlite. Geoscience Frontiers, 13(5), 101429. https://doi.org/10.1016/j.gsf.2022.101429 .

Gibson S.A., Thompson R.N., Leonardos O.H., Dickin A.P., Mitchell L.G. 1995. The Late cretaceous impact of the Trindade mantle plume: evidence from large volume, mafic, potassic magmatism in southeastern Brazil. Journal of Petrology, 36(1), 189-229. https://doi.org/10.1093/petrology/36.1.189 .

Giuliani A., Pearson D.G. 2019. Kimberlites: from deep Earth to Diamond mines. Elements, 15(6), 377-380. https://doi.org/10.2138/gselements.15.6.377 .

Gonzaga G.M., Tompkins L.A. 1991. Geologia do diamante. In: Schobbenhaus C., Queiroz E.T., Coelho C.E.S. Principais depósitos minerais do Brasil. Brasília, DNPM, Companhia Vale do Rio Doce, 4, 53-116.

Griffin W.L., Fisher N.I., Friedman J.H., Ryan C.G., O'Reilly S.Y. 1999. Cr-pyrope garnets in the lithospheric mantle,1, Compositional systematics and relations to tectonic setting. Journal of Petrology, 40(5), 679–704. https://doi.org/10.1093/petroj/40.5.679 .

Grütter H.S., Gurney J.J., Menzies A.H., Winter F. 2004. An update classification scheme for mantle-derived garnet for use by diamond explores. Lithos, 77(1-4), 841-857. https://doi.org/10.1016/j.lithos.2004.04.012 .

Guarino V., Wu F.-Y., Lustrino M., Melluso L., Brotzu P., Gomes C.B., Ruberti E., Tassinari C.C.G., Svisero D.P. 2013. U-Pb ages, Sr-Nd-isotope geochemistry, and petrogenesis of kimberlites, kamafugites and phlogopite-picrites of the Alto Paranaíba Igneous Province, Brazil. Chemical Geology, 353(30), 65-82. https://doi.org/10.1016/j.chemgeo.2012.06.016 .

Guo P., Xu W.-L., Wang, C-.G., Zhang Y.-L. 2019. Thermal state and structure of lithospheric mantle beneath the Xing'an Massif, northeast China: constraints from mantle xenoliths entrained by Cenozoic basalts. Geological Journal, 54(6), 3226-3238. https://doi.org/10.1002/gj.3322 .

Hasterok D., Chapman D.S. 2011. Heat production and geotherms for the continental lithosphere. Earth and Planetary Science Letters, 307(1-2), 59–70. https://doi.org/10.1016/j.epsl.2011.04.034 .

Heaman L.M., Teixeira N.A., Gobbo L., Gaspar J.C. 1998. U-Pb mantle zircon ages for kimberlites from the Juína and Paranatinga Provinces, Brazil. In: International Kimberlite Conference, 7, 322-324. https://doi.org/10.29173/ikc2723 .

Hill P.J.A., Kopylova M., Russel J.K., Cookenboo H. 2015. Mineralogical controls on garnet composition in the cratonic mantle. Contributions

to Mineralogy and Petrology, 169(2), 1-20. http://dx.doi.org/10.1007/s00410-014-1102-7 .

Holwell D.A., Fiorentini M., McDonald I., Lu Y., Giuliani A., Smith D.J., Keith M., Locmelis M. 2019. A metasomatized lithospheric mantle control on the metallogenic signature of post-subduction magmatism. Nature communications, 10, 3511. https://doi.org/10.1038/s41467-019-11065-4 .

Hunt L., Stachel T., Morton R., Grütter H., Creaser R.A. 2009. The Carolina kimberlite, Brazil – Insights into an unconventional diamond deposit. Lithos 112(2), 843–851. https://doi.org/10.1016/j.lithos.2009.04.018 .

Hutchison W., Finch A.A., Borst A.M., Marks M.A.W., Upton B.G.J., Zerkle A.L., Stüeken E.E., Boyce A.J. 2021. Mantle sources and magma evolution in Europe´s largest rare earth element belt (Gardar Province, SW Greenland): new insights from sulfur isotopes. Earth and Planetary Science Letters, 568, 117034. https://doi.org/10.1016/j.epsl.2021.117034 .

Junqueira-Brod T.C., Roig H.L., Gaspar J.C., Brod J.A., Meneses P.R. 2002. A Província Alcalina de Goiás e a extensão do seu vulcanismo kamafugítico. Revista Brasileira de Geociências, 32(4), 559-566. Available online at: https://www.ppegeo.igc.usp.br/index.php/rbg/article/view/9853/9825 / (accessed on 26 October 2022).

Kaminsky F.V., Khachatryan G.K., Andreazza P., Araujo D., Griffin W.L. 2008. Super-deep diamonds from kimberlites in the Juina area, Mato Grosso State, Brazil. In: International Kimberlite Conference, 9, 9IKC-A-00005. https://doi.org/10.29173/ikc3257 .

Kaminsky F.V., Sablukov S.M., Belousova E.A., Andreazza P., Tremblay M., Griffin W.L. 2010. Kimberlitic sources of super-deep diamonds in the Juína area, Mato Grosso state, Brazil. Lithos, 114 (1-2), 16-29. https://doi.org/10.1016/j.lithos.2009.07.012 .

Karfunkel J., Hoover D., Fernandes A.F., Sgarbi G.N.C., Kambrock K., Oliveira G.D. 2014. Diamonds from the Corormandel area, West Minas Gerais state, Brazil: an update and new data on surface sources and origin. Brazilian Journal of Geology, 44(2), 325-338. https://doi.org/10.5327/Z2317-4889201400020011 .

Klein-BenDavid O., Pearson D.G. 2009. Origins of subcalcic garnets and their relation to diamond forming fluid – Case studies from Ekati (NWT-Canada) and Murowa (Zimbabwe). Geochimica et Cosmochimica Acta, 73(3), 837-855. https://doi.org/10.1016/j.gca.2008.04.044 .

Leonardos O.H., Carvalho J.B., Tallarico F.H.B., Gibson S.A., Thompson R.N., Meyer H.O.A., Dickin A.P. 1993. O xenólito de granada lherzolito de Três Ranchos 4: uma rocha matriz do diamante na província magmática cretácea do Alto Paranaíba, Goiás. In: Weska R., Leonardos O.H., Gonzaga G.M. (eds.). Simpósio Brasileiro de Geologia do Diamante, 1, Publicação Especial-UFMT 2/93, 3-16.

Locock A.J. 2008. An excel spreadsheet to recast analyses of garnet into end-member components, and a synopsis of the crystal chemistry of natural silicate garnets. Computer & Geosciences, 34(12), 1769-1780. https://doi.org/10.1016/j.cageo.2007.12.013 .

Marques L.S., Rocha-Júnior E.R.V., Babinski M., Carvas K.Z., Petronilho L.A., De Min A. 2016. Lead isotope constraints on the mantle sources involved in the genesis of Mesozoic high-Ti tholeiite dykes (Urubici type) from the São Francisco Craton (Southern Espinhaço, Brazil). Brazilian Journal of Geology, 46, Supl. 1, 105-122. https://doi.org/10.1590/2317-4889201620150010 .

Masun K.M., Scott-Smith B.H. 2008. The Pimenta Bueno kimberlite field, Rondônia, Brazil: Tuffisitic kimberlite and transitional textures. Journal of Volcanology and Geothermal Research, 174(1-3), 81-89. https://doi.org/10.1016/j.jvolgeores.2007.12.043

Maunula T. 2006. Technical report of the Pimenta Bueno Project, Brazil to Vaaldiam Resources Ltd, 87 p.

Melluso L., Lustrino M., Ruberti E., Brotzu P., Gomes C.B., Morbidelli L., Morra V., Svisero D.P. 2008. Major- and trace-element composition of olivine, perovskite, clinopyroxene, Cr-Fe-Ti oxides, phlogopite and host kamafugites and kimberlites, Alto Paranaiba, Brazil. Canadian Mineralogist, 46(1), 19-40. https://doi.org/10.3749/canmin.46.1.19 .

Meyer H.O.A., Svisero D.P. 1991. Limeira and Indaiá intrusions, Minas Gerais. Field Guide Book. In: International Kimberlite Conference, 5, 49-55.

Morimoto N. 1988. Nomenclature of pyroxenes. Mineralogy and Petrology, 39, 55-76. https://doi.org/10.1007/BF01226262 .

Nannini F. 2011. Petrografia e química mineral de xenólitos mantélicos da intrusão Kimberlítica Indaía, Monte Carmelo, MG. MSc Dissertation, Instituto de Geociências, Universidade de São Paulo, São Paulo, 100 p. https://doi.org/10.11606/D.44.2011.tde-17082011-111449 .

Nannini F. 2016. Geologia e petrologia de xenólitos mantélicos da Província Ígnea do Alto Paranaíba, Minas Gerais. PhD Thesis, Instituto de Geociências, Universidade de São Paulo, São Paulo, 288 p. https://doi.org/10.11606/T.44.2016.tde-04052016-112733 .

Nannini F., Cabral Neto I., Silveira F.V., Cunha L.M., Oliveira R.G., Weska R.K. 2017. Áreas kimberlíticas e diamantíferas do estado do Mato Grosso. Informe de Recursos Minerais, Série Pedras Preciosas, 12, Brasília, CPRM, 42 p. Available online at: https://rigeo.cprm.gov.br/handle/doc/17618 / (accessed on 26 October 2022).

Navon O., Wirth R., Schmidt C., Jablon B.M., Schreiber A., Emmanuel S. 2017. Solid molecular nitrogen (δ-N2) inclusions in Juina diamonds: Exsolution at the base of the transition zone. Earth and Planetary Science Letters, 464, 237-247. https://doi.org/10.1016/j.epsl.2017.01.035 .

Nickel K.G., Green D.H. 1985. Empirical geothermobarometry for garnet peridotites and implications for the nature of the lithosphere, kimberlites and diamonds. Earth and Planetary Science Letters, 73(1), 158-170. https://doi.org/10.1016/0012-821X(85)90043-3 .

Nimis P., Taylor W.R. 2000. Single clinopyroxene thermobarometry for garnet peridotites. Part I. Calibration and testing of a Cr-in Cpx barometer and an enstatite-in-Cpx thermometer. Contributions to Mineralogy and Petrology, 139(5), 541-554. http://dx.doi.org/10.1007/s004100000156 .

Nimis P., Grutter H. 2010. Internally consistent geothermometers for garnet peridotites and pyroxenites. Contributions to Mineralogy and Petrology, 159(3), 411-427. http://dx.doi.org/10.1007/s00410-009-0455-9 .

Oliveira A.M., Leahy G.A.S., Rios D.C., Marques A.S.C.S., Conceição H. 2019. Minerais indicadores de kimberlitos: as granadas do pipe Carolina-1, estado de Rondônia. In: Simpósio de Geologia do Nordeste, 28, 332. Available online at: http://sbgeo.org.br/assets/admin/imgCk/files/Anais/Anais_28o_Simposio_de_Geologia_do_Nordeste-ISBN.pdf / (accessed on 26 October 2022).

Pasin D.A.B. 2008. Alteração hidrotermal nos kimberlitos do distrito diamantífero de Coromandel, Minas gerais, Brasil. PhD Thesis, Instituto de Geociências, Universidade Federal do Rio de Janeiro, 236 p.

Pearson D.G., Canil D., Shirey S.B. 2014a. 3.5 — mantle samples included in volcanic rocks: xenoliths and diamonds. In: Holland H.D., Turekian K.K. (eds). Treatise on Geochemistry. 2nd ed. Oxford, Elsevier, p. 169–253.

Pearson D.G., Brenker F.E., Nestola F., McNeill J., Nasdala L., Hutchinson M.T., Matveev S., Mather K., Silversmit G., Schmitz S., Vekemans B., Vincze L. 2014b. Hydrous mantle transition zone indicated by ringwoodite included within diamond. Nature, 507(7491), 221-224. https://doi.org/10.1038/nature13080 .

Pereira R.S., Fuck R.A. 2005. Archean Nucleii and the distribution of kimberlite and related rocks in the São Francisco Craton, Brazil. Revista Brasileira de Geociências 35(4), 297-310. Available online at: https://www.ppegeo.igc.usp.br/index.php/rbg/article/view/9405/9904 / (accessed on 27 October 2022).

Pereira R.S., Fuck R.A., França O.S., Leite A.A. 2017. Evidence of young, proximal and primary (YPP) diamond source occuring in alluviums in the Santo Antônio do Bonito, Santo Inácio and Douradinho rivers in Coromandel region, Minas Gerais. Brazilian Journal of Geology, 47(3), 383-401. https://doi.org/10.1590/2317-4889201720170047 .

Pintér Z., Patkó L., Djoukam J.F.T., Kovács I., Tchouankoue J.P., Falus G., Konc Z., Tommasi A., Barou F., Mihály J., Németh C., Jeffries T. 2015. Characterization of the sub-continental lithospheric mantle beneath the Cameroon volcanic line inferred from alkaline basalt hosted peridotite xenoliths from Barombi Mbo and Nyos Lakes. Journal of African Earth Sciences, 111, 170-193. https://doi.org/10.1016/j.jafrearsci.2015.07.006 .

Pinto L.G.R. 2009. Interpretação de dados gravimétricos e eletromagnéticos do sul do cráton São Francisco: novos modelos crustais e litosféricos. PhD Thesis, Instituto de Astronomia, Universidade de São Paulo, São Paulo, 145 p. https://doi.org/10.11606/T.14.2019.tde-25052018-081155 .

Powell R. 1985 Regression diagnostics and robust regress in geothermometer/geobarometer calibration: the garnet-clinopyroxene geothermometer revisited. Journal of Metamorphic Geology, 3(3), 231-243. https://doi.org/10.1111/j.1525-1314.1985.tb00319.x .

Quadros M.L.E.S., Rizzotto G.J. 2007. Geologia e recursos minerais do Estado de Rondônia. Porto Velho, CPRM, 153 p. Available online at: https://rigeo.cprm.gov.br/handle/doc/10277 / (accessed on 27 October 2022).

Ramsay R.R. 1992. Geochemistry of diamond indicator minerals. PhD Thesis, University of Western Australia, Perth.

Read G., Grütter H., Winter S., Luckman N., Gaunt F., Thomsen F. 2004. Stratigraphic relations, kimberlite emplacement and lithospheric thermal evolution, Quiricó basin, Minas Gerais State, Brazil. Lithos, 77, 803-818. https://doi.org/10.1016/j.lithos.2004.04.011

Richard L.R. 1995. Mineralogical and petrological data processing system. Minpet for Windows, version 2.02. MinPet Geological Software, Canadá.

Rocha L.M. 2013. Caracterização magnética da porção central do lineamento 125º. PhD Thesis, Instituto de Geociências, Universidade de Brasília, Brasília, 166 p. Available online at: https://repositorio.unb.br/handle/10482/15699 / (accessed on 26 October 2022).

Rocha L.G.M., Correa R., Silva A., Matos D. 2019. Geophysical reassessment of the Azimuth 125º Lineament: emplacement model and propagation of its dikes. Journal of the Geological Survey of Brazil, 2(1), 87-98. https://doi.org/10.29396/jgsb.2019.v2.n1.6 .

Rudloff-Grund J., Brenker F.E., Marquardt K., Howell D., Schreiber A., O´Reilly S.Y., Griffin W.L., Kaminsky F.V. 2016. Nitrogen nanoinclusions in milky diamonds from Juina area, Mato Grosso state, Brazil. Lithos, 265, 57-67. https://doi.org/10.1016/j.lithos.2016.09.022 .

Stachel T., Harris J.W. 2008. The origin of cratonic diamonds – Constraints from mineral inclusions. Ore Geology Reviews, 34(1-2), 5-32. https://doi.org/10.1016/j.oregeorev.2007.05.002 .

Simakov S., Dolivo-Dobrovolsky M. 2009. PTQuick. Versions 1.4.0.5 (PTQuick.exe), 1.4.0.12 (PTools.dll). Available online at: http://dimadd.ru/en/Programs/ptquick / (accessed on 31 October 2022).

Silva S. 2008. Petrografia e química mineral das intrusões Indaiá I e Indaiá II, oeste do estado de Minas Gerais. MSc Dissertatiton, Instituto de Geociências, Universidade de São Paulo, São Paulo, 113 p. https://doi.org/10.11606/D.44.2008.tde-15082008-145504 .

Sobolev N.V., Lavrent'yev Y.G., Pokhilenko N.P., Usova L.V. 1973. Chrome-rich garnets from the kimberlites of Yakutia and their paragenesis. Contributions to Mineralogy and Petrology, 40, 39-52.

Streckeisen A. 1973. Plutonic Rocks. Classification and nomenclature recommended by the IUGS subcommission on the sistematics of igneous rocks. Geotimes, 18(10), 26–30.

Svisero D.P. 1995. Distribution and origin of diamonds in Brazil: an overview. Journal of Geodynamics, 20(4), 493-514. https://doi.org/10.1016/0264-3707(95)00017-4 .

Sudholz Z.J., Yaxley G.M., Jaques A.L., Brey G.P. 2021. Experimental recalibration of the Cr-in-clinopyroxene geobarometer: improved precision and reliability above 4.5 Gpa. Contributions to Mineralogy and Petrology, 176, 11. https://doi.org/10.1007/s00410-020-01768-z .

Tappert R., Stachel T., Harris J.W., Muehlenbachs K., Brey G.P. 2006. Placer diamonds from Brazil: indicators of the composition of the Earth's mantle and the distance to their kimberlitic sources. Economic Geology, 101(2), 453–470. https://doi.org/10.2113/gsecongeo.101.2.453 .

Tassinari C.C.G., Macambira M.J.B. 1999. Geochronological Provinces of the Amazonian Craton. Episodes, 22(3), 174-182. https://doi.org/10.18814/epiiugs/1999/v22i3/004 .

Thomaz L.V. 2009. Estudo petrográfico e química mineral da intrusão kimberlítica Régis, no oeste de Minas Gerais. MSc Dissertatiton, Instituto de Geociências, Universidade de São Paulo, São Paulo, 143 p. https://doi.org/10.11606/D.44.2009.tde-19082009-094419 .

Thomson A.R., Kohn S.C., Bulanova G.P., Smith C.B., Araujo D., Walter M.J. 2016. Trace element composition of silicate inclusions in sub-lithospheric Diamonds from the Juina-5 kimberlite: Evidence for Diamond growth from slab melts. Lithos, 265, 108-124. https://doi.org/10.1016/j.lithos.2016.08.035 .

Weska R.K., Svisero D.P. 2001. Aspectos geológicos de algumas intrusões kimberlíticas da região de Paranatinga, Mato Grosso. Revista Brasileira de Geociências, 31(4), 555-562. Available online at: https://ppegeo.igc.usp.br/index.php/rbg/article/view/10623 / (accessed on 27 October 2022).

Weska R.K., Brod J.A., Dantas E.L., Araújo D.P. 2012. Mineral chemistry of garnets and ilmenites of the Pepper-1 and Cosmos-3 intrusions, Espigão d'Oeste, Rondônia, Brazil. In: International Kimberlite Conference, 10, 273. https://doi.org/10.29173/ikc3780 .

Yavuz F. 2013. WinPyrox: A Windows program for pyroxene calculation classification and thermobarometry. American Mineralogist, 98, 1338-1359. https://doi.org/10.2138/am.2013.4292 .

Yavuz F., Yildirim D.K. 2020. WinGrt, a Windows program for garnet supergroup minerals. Journal of Geosciences, 65(2), 71-95. https://doi.org/10.3190/jgeosci.303 .

Zaffari G.L., Ruiz A.S., Vidotti R.M., Campos F.A.P. 2018. Controle litoestrutural e caracterização geofísica do Complexo Alcalino Planalto da Serra, Mato Grosso. Geologia USP, Série Científica, 18(4), 3-8. https://doi.org/10.11606/issn.2316-9095.v18-152318 .